Changes in apparent temperature and $PM_{2.5}$ around the Beijing-Tianjin megalopolis under greenhouse gas and stratospheric aerosol injection scenarios

Jun Wang[1], John C. Moore[1,2*], Liyun Zhao[1*]
[1]College of Global Change and Earth Systems Science, Beijing Normal University, Beijing 100875, China
[2]Arctic Center, University of Lapland, Rovaniemi, Finland
Correspondence to: zhaoliyun@bnu.edu.cn, john.moore.bnu@gmail.com

Abstract. Apparent temperatures (AP) and ground level aerosol pollution ($PM_{2.5}$) are important factors in human health, particularly in rapidly growing urban centres in the developing world. We ~~compare~~ quantify how changes in apparent temperature~~s~~ – that is a combination of 2 m air temperature, relative humidity and surface wind speed, and $PM_{2.5}$ concentrations – that depend on the same meteorological factors along with future industrial emission policy, may impact people in the greater Beijing region. ~~in f~~Four Earth System Models (ESM) ~~under~~ simulations of the modest greenhouse emissions RCP4.5, the "business-as-usual" RCP8.5 and the stratospheric aerosol injection G4 geoengineering scenarios~~. Apparent temperatures come from both~~ are downscaled using both a 10 ~~–~~km resolution dynamic~~ally downscaled~~ model (WRF), and a statistically ~~bias corrected~~approach (ISIMIP). We use multiple linear regression models to simulate changes in $PM_{2.5}$ and the contributions meteorological factors make in controlling seasonal AP and $PM_{2.5}$. ~~and downscaled simulation for the greater Beijing region. ISIMIP downscaling method tends to simulate apparent temperatures well at present in all seasons, and WRF produces warmer winters than does ISIMIP.~~ WRF produces warmer winters and cooler summers than does ISIMIP both now and in the future. These differences mean that estimates of numbers of days with extreme apparent temperatures vary systematically with downscaling method, as well as between climate models and scenarios. Air temperature changes dominate differences in apparent temperatures between future scenarios even more than they do at present because the reductions in humidity expected under solar geoengineering are overwhelmed by rising vapor pressure due to rising temperatures and the lower windspeeds expected in the region in all future scenarios. Temperature and humidity differences between scenarios change the relative risk of disease from $PM_{2.5}$ such that G4 results in 1-3% higher health risks than RCP4.5. Urban centres see larger rises in extreme apparent temperatures than rural surroundings due to differences in land surface type, and since these are also the most densely populated, health impacts will be dominated by the larger rises in apparent temperatures in these urban areas.

500 character non-technical text

Apparent temperatures and $PM_{2.5}$ pollution depends on~~that include~~ humidity and wind speed in addition to surface temperature ~~measure~~ and impacts human ~~heat stress~~health and comfort. ~~We show that a~~Apparent temperatures will reach dangerous levels more commonly in future ~~and rise faster than air temperatures~~ because of water vapor pressure rises and lower expected wind speeds~~.~~, but these will also drive change in $PM_{2.5}$. Solar geoengineering can reduce the frequency of extreme events significantly relative to modest, and especially "business as usual" greenhouse scenarios.

1. Introduction

Global mean surface temperature has increased by 0.92°C (0.68-1.17°C) during 1880-2012 (IPCC, 2021), which naturally also impacts the human living environment (Kraaijenbrink et al., 2017; Garcia et al., 2018). However, neither land surface temperature nor near-surface air temperature can adequately represent the temperature we experience. Apparent temperature (AP), that is how the temperature feels, is formulated to reflect human thermal comfort and is probably a more important indication of health than daily maximum or minimum temperatures (Fischer et al., 2013; Matthews et al., 2017; Wang et al., 2021). There are various approaches to estimating how the weather conditions affect comfort, but apparent temperature is governed by air temperature, humidity and wind speed (Steadman 1984; Steadman 1994). These are known empirically to affect human thermal comfort (Jacobs et al., 2013), and thresholds have been designed to indicate danger and health risks under extreme heat events (Ho et al., 2016). Analysis of historical apparent temperatures in China (Wu et al., 2017; Chi et al., 2018; Wang et al., 2019), Australia (Jacobs et al., 2013), and the USA (Grundstein et al., 2011) all find that apparent temperature is increasing faster than air temperature. This is due to both decreasing wind speeds and, especially to increasing vapor pressure (Song et al., 2022).

As the world warms, apparent temperature is expected to rise faster than air temperatures in the future (Li et al., 2018; Song et al., 2022). Hence, humans, and other species, will face more heat-related stress but less cold-related environmental stress in the warmer future (Wang et al., 2018; Zhu et al., 2019). Since most of the population is now urban, the conditions in cities will determine how tolerable are future climates for much of humanity, while the differences in thermal comfort between urbanized and rural regions will be a factor in driving urbanization. Reliable estimates of future urban temperatures and their rural surroundings require methods to improve on standard climate model resolution to adequately represent the different land surface types; especially the rapid and accelerating changes in land cover in the huge urban areas characteristic of sprawling developments in the developing world. This is usually done with either statistical or dynamic downscaling approaches, and in this article we examine both methods.

In early 2013, Beijing encountered a serious pollution incident. The concentration of $PM_{2.5}$ (particles with diameters less than or equal to 2.5 μm in the atmosphere) exceeded 500 μg/m^3 (Wang et al., 2014). Following this event and its expected impacts on human health (Guan et al., 2016; Fan et al., 2021) and the economy (Maji et al., 2018; Wang et al., 2020), the Beijing municipal government launched the Clean Air Action Plan in 2013. The annual mean concentration of $PM_{2.5}$ in Beijing-Tianjin-Hebei region decreased from 90.6 μg/m^3 in 2013 to 56.3 μg/m^3 in 2017, a decrease of about 38% (Zhang et al., 2019), although this is still more than double the EU air quality standard (25 μg/m^3) and above the Chinese FGNS (First Grand National Standard) of 35 μg/m^3. The concentration of $PM_{2.5}$ is related to anthropogenic emissions, but also dependent on meteorological conditions (Chen et al., 2020). Simulations suggested that 80% of the 2013-2017 lowering of $PM_{2.5}$ concentration came from emission reductions in Beijing (Chen et al. 2019). Humidity and temperature are the main meteorological factors affecting $PM_{2.5}$ concentration in Beijing in summer, while humidity and wind speed are the main factors in winter (Chen et al., 2018). Simulations driven by different RCP emission scenarios with fixed meteorology for the year 2010 suggest that $PM_{2.5}$ concentration will meet FGNS under RCP2.6, RCP4.5 and RCP8.5 in Beijing-Tianjin-Hebei after 2040 (Li et al., 2016).

The focus here is in the differences in apparent temperature and $PM_{2.5}$ that may arise from solar geoengineering (that is reduction in incoming short-wave radiation to offset longwave absorption by greenhouse gases) via stratospheric aerosol injection (SAI), and pure greenhouse gas climates. We use all four climate models that have provided sufficient data from the G4 scenario described by the Geoengineering Model Intercomparison Project (GeoMIP). G4 specifies sulfates as the aerosol, and greenhouse gas emissions from the RCP4.5 scenario (Kravitz et al., 2011). The impacts of G4 on surface temperature and precipitation have been discussed at regional scales (Yu et al., 2015) and both are lowered relative to RCP4.5. Some studies have focused on regional impact of SAI on apparent or wet bulb temperatures: in Europe, (Jones et al., 2018); East Asia (Kim et al., 2020); and the Maritime Continent (Kuswanto et al., 2021). But none of these studies have considered apparent temperature at scales appropriate for rapidly urbanizing regions such as on the North China Plain. The only study to date on SAI impacts on $PM_{2.5}$ pollution was a coarse resolution (4°×5°) global scale model with sophisticated chemistry (Eastham et al., 2018). They simulated aerosol rainout from the stratosphere to ground level, leading to an eventual increase in ground level $PM_{2.5}$. Eastham et al. (2018) concluded that SAI changes in tropospheric and stratospheric ozone dominated $PM_{2.5}$ impacts on global mortality. However, this study did not consider meteorological effects nor the situation in a highly polluted urban environment such as included in our domain, and which is typical of much of the developing world.

The greater Beijing megalopolis lies in complex terrain, surrounded by hills and mountains on three sides, and a flat plain to the southeast coast (Fig. 1). Over the period ~~1978~~1971-~~2008~~2014, ~~Beijing experienced an increasing trend of 12.7% or 2.07 days~~

~~per decade in extreme warm nights (Wang et al., 2013), and urbanization produced an average increase in temperature of approximately 0.60°C.~~apparent temperature rose at a rate of 0.42°C/10 years over Beijing-Tianjin-Hebei region, with urbanization having an effect of 0.12°C/10 years (Luo and Lau, 2021). By the end of 2019, the permanent resident population in Beijing exceeded 21 million. Tianjin, 100 km from Beijing, is the fourth largest city in China with a population of about 15 million, and Langfang (population 4 million) is about 50 km from Beijing. Thus, the region contains a comparable urbanized population as the northeast US megalopolis. Since its climate is characterized by hot and moist summer monsoon conditions, the population is at an enhanced risk as urban heat island effects lead to city temperatures warming faster than their rural counterparts.

There are large uncertainties in projecting $PM_{2.5}$ concentration in the future due to both climate and industrial policies. Statistical methods are much faster than atmospheric chemistry models (Mishra et al., 2015), and different scenarios are easy to implement. We use a Multiple Linear Regression (MLR) model to establish the links between $PM_{2.5}$ concentration, meteorology and emissions (Upadhyay et al., 2018; Tong et al., 2018). We project and compare the differences of $PM_{2.5}$ concentration under G4 and RCP4.5 scenarios, and between different $PM_{2.5}$ emission scenarios.

Accurate meteorological data are crucial in simulating future apparent temperatures and $PM_{2.5}$ because all ESM suffer from bias, and this problem is especially egregious at small scales. A companion paper (Wang et al., 2022~~ in review~~) looked at differences between downscaling methods with the same 4 Earth System Models (ESM), domain and scenarios as we use here.

In this paper, we use the downscaled data to explore the effect of SAI on apparent temperature and $PM_{2.5}$ over the greater Beijing megalopolis. The paper is organized as follows. The data~~, –~~ and methods of calculating AP~~ and~~, AP thresholds, the $PM_{2.5}$ MLR model and its validation are briefly described in Section 2. The results from present day simulation and future projections on apparent temperature and $PM_{2.5}$ are given in Section 3, along with their associated impact ~~analysis~~analyses. In ~~Finally, ~~Section 4 we discuss~~es~~ and interpret the findings, and finally we conclude~~s the study~~ with a summary of the main implications of the geoengineering impacts on these two important human health indices in Section 5.

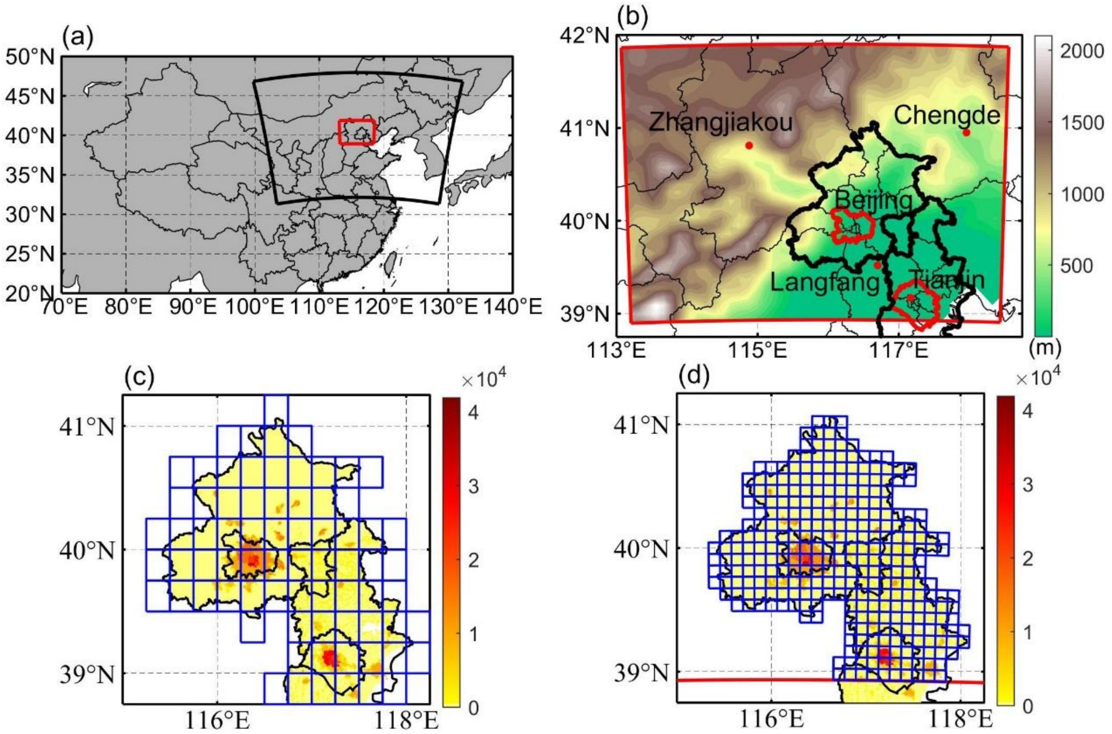

Figure 1. a, The 10 km WRF domain (red box) nested inside a 30 km resolution WRF domain (large black sector). **b,** The inner domain topography and major conurbations (red dots), with the urban areas of Beijing and Tianjin enclosed in red curves. Panels c and d show the population density (persons per km^2) of Beijing and Tianjin provinces (defined by black borders) in 2010 and the grid cells within the Beijing-Tianjin province (blue boxes) when downscaled by ISIMIP **(c)** and WRF **(d)**.

2. Data and Methods

2.1 Scenarios, ESM, downscaling methods and bias correction

The scenarios, ESM, downscaling methods and bias correction methods we use here are as described in detail by Wang et al., (~~in review,~~ 2022), and we just summarize the method briefly here. We use three different scenarios: RCP4.5 and RCP8.5 (Riahi et al., 2011) and the GeoMIP G4 scenario which span a useful range of climate scenarios: RCP4.5 is similar (Vandyck et al., 2016) to the expected trajectory of emissions under the 2015 Paris Climate Accord agreed Nationally Determined Contributions (NDCs); RCP8.5 represents a formerly business-as-usual, no climate mitigation policies, large signal to noise ratio scenario; G4 represents a similar radiative forcing as produced by the 1991 Mount Pinatubo volcanic eruption repeating every 4 years.

Climate simulations are performed by~~forcing comes from~~ 4 ESM: BNU-ESM (Ji et al., 2014), HadGEM2-ES (Collins et al., 2011), MIROC-ESM (Watanabe et al., 2011) and MIROC-ESM-CHEM (Watanabe et al., 2011). We compare dynamical and statistical downscaling methods to convert the ESM data to scales more suited to capturing differences between contrasting rural and urban environments. To validate the downscaled AP from model results, we use the daily temperature, humidity and wind speed during 2008-2017 from the gridded observational dataset CN05.1 with the resolution of 0.25°× 0.25° based on the observational data from more than 2400 surface meteorological stations in China, which are interpolated using the "anomaly approach" (Wu and Gao, 2013). This dataset is widely used, and has good performance relative to other reanalysis datasets over China (Zhou et al., 2016; Yang et al., 2019; Yang et al., 2023; Yang and Tang, 2023)~~The observational data set we use to assess the performance of two downscaling methods is the daily ERA5 (Hersbach et al., 2018) reanalysis data with a resolution of 0.25°×0.25° over the domain in Fig. 1b during 2008-2017~~. Dynamical downscaling for the 4 ESM datasets was done with WRFv.3.9.1 with a parameter set used for urban China studies (Wang et al., 2012) in two nested domains at 30 and 10 km resolution over 2 time slices (2008-2017 and 2060-2069). We corrected the biases in WRF output using the quantile delta mapping method (QDM; Wilcke et al., 2013) with ERA5 (Hersbach et al., 2018) to preserve the mean probability density function of the output over the domain without degrading the WRF spatial pattern. All WRF results presented are after QDM bias correction. Statistical downscaling was done with the trend-preserving statistical bias-correction Inter-Sectoral Impact Model Intercomparison Project (ISIMIP) method (Hempel et al., 2013) for the raw ESM output, producing output matching the mean ERA5 observational data in the reference historical period with the same spatial resolution, while allowing the individual ESM trends in each variable to be preserved.

2.2 $PM_{2.5}$ concentration and emission data

In China there were few $PM_{2.5}$ monitoring stations before 2013 (Xue et al., 2021). However, aerosol optical depths produced by the Moderate Resolution Imaging Spectroradiometer (MODIS) have been used to build a daily $PM_{2.5}$ concentration dataset (ChinaHighPM2.5) at 1 km resolution from 2000 to 2018 (Wei et al., 2020). We use monthly $PM_{2.5}$ concentration data during 2008-2015 from ChinaHighPM2.5 to train the MLR model, and the data during 2016-2017 to validate it. Figure S1 shows annual $PM_{2.5}$ concentration over Beijing areas during 2008 (a) and 2017 (b).

Recent gridded monthly $PM_{2.5}$ emission data were derived from the Hemispheric Transport of Air Pollution (HTAP_V3) with a resolution of 0.1°×0.1° during 2008-2017, which is a widely used anthropogenic emission dataset (Janssens-Maenhout et al., 2015). $PM_{2.5}$ emissions over Beijing areas during 2008 (c) and 2017 (d) are shown in Fig. S1.

Future gridded monthly $PM_{2.5}$ emissions to 2050 are available in the ECLIPSE V6b database (Stohl et al., 2015), generated by the GAINS (Greenhouse gas Air pollution Interactions and Synergies) model (Klimont et al., 2017). The ECLIPSE V6b baseline emission scenario assumes that future anthropogenic emissions are consistent with those under current environmental policies, hence it is the "worst" scenario without considering any mitigation measures (Li et al., 2018; Nguyen et al., 2020). Projected emissions are shown in Fig S2, with emissions plateauing at ~40 kt/year after 2030, so we assume 2060s levels are similar. These ECLIPSE projections are significantly larger than present day estimates from HTAP_V3. We therefore estimate 2060s emissions as the recent gridded monthly $PM_{2.5}$ emissions from HTAP_V3 scaled by the ratios of 2050 ECLIPSE emission to average annual emissions between 2010 and 2015. Before processing data, $PM_{2.5}$ concentration is bilinearly interpolated to the WRF and ISIMIP grids, while $PM_{2.5}$ emissions are conservatively interpolated to the target grids.

2.~~2~~ 3 Apparent temperature

We use the formula proposed in Steadman (1984) to estimate apparent temperature under shade, which has been widely used to study heat waves, heat stress and temperature-related mortality (Perkins and Alexander, 2013; Lyon and Barnston, 2017; Lee and Sheridan, 2018; Zhu et al., 2021):

$$AP = -2.7 + 1.04 \times T + 2 \times P - 0.65 \times W \qquad (1)$$

where AP is the apparent temperature (°C) under shade meaning that radiation is not considered; T is the 2 m temperature (°C), W is the wind speed at 10 m above the ground (m/s), and P is the vapor pressure (kPa) calculated by

$$P = P_s \times RH \qquad (2)$$

where P_s is the saturation vapor pressure (kPa), and RH is the relative humidity (%). P_s is calculated using the ~~Clausius–Clapeyron relation~~Tetens empirical formula (Murray, 1966):

$$P_s = \begin{cases} 0.61078 \times e^{\left(\frac{17.2693882 \times T}{T+237.3}\right)}, & T \geq 0 \\ 0.61078 \times e^{\left(\frac{21.8745584 \times (T-3)}{T+265.5}\right)}, & T < 0 \end{cases} \qquad (3)$$

To assess the potential risks of heat-related exposure from apparent temperature, we also count the number of days with AP > 32°C (NdAP_32) in the Beijing-Tianjin province (Table S1). This threshold does not lead to extreme risk and death, instead it is classified as requiring “extreme caution” by the US National Weather Service (National Weather Service Weather Forecast Office, *https://www.weather.gov/ama/heatindex*), but carries risks of heatstroke, cramps and exhaustion. A threshold of 39°C is classed as “dangerous” and risks heatstroke. While hotter AP thresholds would give a more direct estimate of health risks, the statistics of these presently rare events mean that detecting differences between scenarios is less reliable than using the cooler NdAP_32 threshold simply because the likelihood of rare events are more difficult to accurately quantify than more common events that are sampled more frequently. There is evidence that in some distributions, the likelihood of extremes will increase more rapidly than central parts of a probability distribution, for example large Atlantic hurricanes increasing faster than smaller ones (Grinsted et al., 2013). But the conservative assumption is that similar differences between scenarios would apply for higher thresholds as lower ones.~~. While hotter AP thresholds would give a more direct estimate of health risks, the statistics of these presently rare events mean that detecting differences between scenarios is less reliable than using the cooler NdAP_32 threshold. We presume that similar differences between scenarios would apply for higher thresholds.~~

2.~~3~~ 4 Population Data Set

Since health impacts are more important where there are more people, we calculate the NdAP_32 weighted by population (Fig. 1c and 1d). We employ gridded population data (Fu et al., 2014; https://doi.org/10.3974/geodb.2014.01.06.V1) with a spatial resolution of 1×1 km collected in 2010. The population density distribution in Beijing and Tianjin provinces with the ISIMIP and WRF grid cells contained are shown in the Fig. 1c and 1d.

2.5 MLR model calibration

Previous studies have shown that wind and humidity are the dominant meteorological variables for $PM_{2.5}$ concentration in region we study (Chen et al., 2020). Hence, we generate an MLR model between $PM_{2.5}$ and temperature (T), relative humidity (H), zonal wind (U), meridional wind (V) and $PM_{2.5}$ emissions (E) at every grid cell as follows:

$$PM2.5 = \sum a_i X_i + b \tag{4}$$

Where $X_{i(i=1,2,3,4,5)}$ are the five factors, a_i are the regression coefficients of the X_i with $PM_{2.5}$, and b is the intercept, which is a constant. We assume that all factors should be included in the regression. All the meteorological variables are from the statistical and dynamical downscaling and bias corrected results during 2008-2017, with the first 8 years used for training model and the second 2 years used for validating model. We train the MLR for the 4 ESMs under statistical and dynamical downscaling in each grid cell separately, thus accounting spatial differences in the weighting of the X_i across the domain. Meteorological variables under G4, RCP4.5 and RCP8.5 during 2060-2069 are used for projection.

The contributions of meteorology and $PM_{2.5}$ emissions on future concentrations are examined by using recent $PM_{2.5}$ emissions (baseline) and future $PM_{2.5}$ emissions (mitigation), and the downscaled climate scenarios. Modeled $PM_{2.5}$ concentration using recent meteorology and $PM_{2.5}$ emissions during 2008-2017 (2010s) is considered as our reference.

2.6 MLR model validation

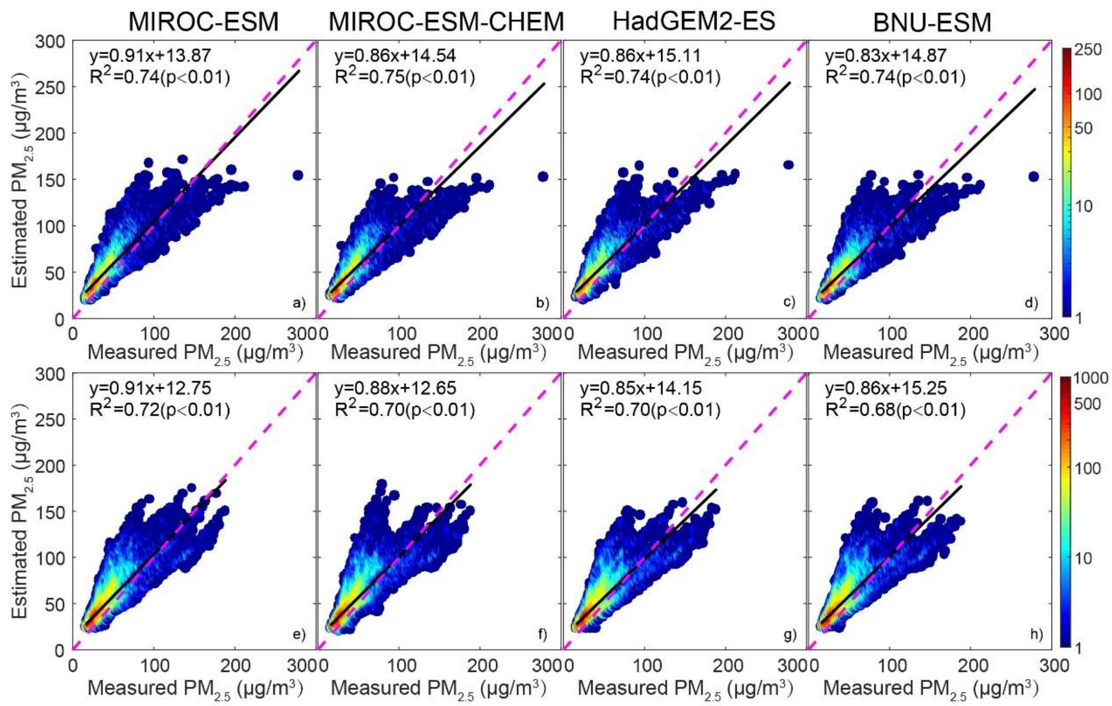

Figure 2. Scatter grams of $PM_{2.5}$ concentration derived by MODIS and estimated by MLR during validation period (2016-2017). Top figures **(a-d)** are the ISIMIP statistical downscaling results, and bottom figures **(e-h)** are the WRF dynamical downscaling results. R^2 means the variance explained by the MLR, and color bar denotes the density of datapoints at integer intervals.

Figure 2 shows the scattergram of $PM_{2.5}$ concentration between ChinaHighPM2.5 dataset and MLR model during validation period based on ISIMIP and WRF results. Observations and MLR models have Pearson's correlations coefficients around 0.86 for ISIMIP results during the validation period, and the coefficient of determination of MLRs are 0.74-0.75 (Fig. 2a-d). WRF Pearson's correlations are slightly lower, 0.82-0.85, and explained variance ranges from 0.68-0.72 (Fig. 2e-h). These results are similar as found by Jin et al. (2022). We also compare the spatial patterns of observed and modeled $PM_{2.5}$ in Fig. S3. Both ISIMIP and WRF results can simulate the distribution characteristics of high concentration of $PM_{2.5}$ in the southeast and low concentration in the northwest.

2.7 Relative risks of mortality related to $PM_{2.5}$

We estimate the effects of $PM_{2.5}$ on mortality by considering changes in the relative risk (RR) of mortality related to $PM_{2.5}$. We lack data on mortality rates in the study domain without which we cannot estimate numbers of fatalities, just the average population-weighted RR. Burnett et al. (2014) established the integrated exposure-response functions we use. The RR is non-linear in concentration, that is an initially low $PM_{2.5}$ region will suffer higher mortality and RR than an initially high $PM_{2.5}$ region if $PM_{2.5}$ is increased by the same amount. Ran et al. (2023) provide RR values for $PM_{2.5}$ concentrations up to 200 μg/m^3 that includes the 5 main major disease endpoints

(Global Burden of Disease Collaborative Network, 2013) of $PM_{2.5}$ related mortality: chronic obstructive pulmonary disease, ischemic heart disease, lung cancer, lung respiratory infection and stroke. We calculate the average population-weighted relative risks based on the gridded population dataset (Section 2.4) and $PM_{2.5}$ concentration in the Beijing-Tianjin province defined in the Fig. 1c-1d, following Ran et al. (2023):

$$RR_{pop,k}=\frac{\sum_{g=1}^{G} POP_g \times RR_k(C_g)}{\sum_{g=1}^{G} POP_g} \qquad (5)$$

$RR_{pop,k}$ is the average population-weighted relative risk of disease k (k=1-5), POP_g is the population of gird g, and $RR_k(C_g)$ is the relative risk of disease k when $PM_{2.5}$ concentration is C_g in the grid of g.

2.~~4~~8 Determination of ~~each factor's~~ contributions to change in AP and $PM_{2.5}$

Equation (1) describes how AP is calculated, and this can be broken down into how much equivalent temperature is produced by each term (Fig. ~~2~~3), with 2008-2017 as the baseline interval for season-by-season contributors to AP. Across scenario seasonal differences in contributors are then calculated as follows. We use an MLR approach, since this minimizes the square differences from the mean across the dataset, with the attendant assumption of independence between the data. Alternatives may also be considered that e.g. minimize the impact of outliers by considering the magnitude of the differences, but we prefer to keep the attractive properties of a least squares approach. ~~We use multiple linear regression to reconstruct the relationship between change~~The dependent variable in the MLR is the change in AP (ΔAP) and the independent variables are changes in each factor for each future scenario,

$$\Delta AP=\sum \alpha\cancel{a}_i X_i+\beta\cancel{b} \qquad (6\cancel{4})$$

where $X_{i(i=1,2,3)}$ are the daily changes of the three meteorological factors between two scenarios: 2 m temperature (ΔT), 2 m relative humidity (ΔRH) and 10 m wind speed (ΔW), $\alpha\cancel{a}_i$ are the regression coefficients of the X_i with ΔAP, and $\beta\cancel{b}$ is the intercept, which is a constant. We assume that all three meteorological factors should be included in the regression and we estimate the contributions of each factor to changes of AP as:

$$\cancel{C}K_i=\frac{\alpha\cancel{a}_i\overline{X}_i}{\sum \cancel{a}\alpha_i \overline{X}_i} \qquad (7\cancel{5})$$

where $\cancel{C}K_{i(i=1,2,3)}$ is the contributions (in units of temperature) from each factor to the changes of the AP, and $\overline{X}_i$ are the mean differences in temperature equivalent due to each factor between two scenarios.

The contribution of changes in each factor in changes of $PM_{2.5}$ is simpler since we assume that the relationship between each factor and $PM_{2.5}$ is linear, and so its contribution is the ratio of product of the regression coefficient and the change of each factor to the change of $PM_{2.5}$.

3. Results

3.1 Recent apparent temperatures

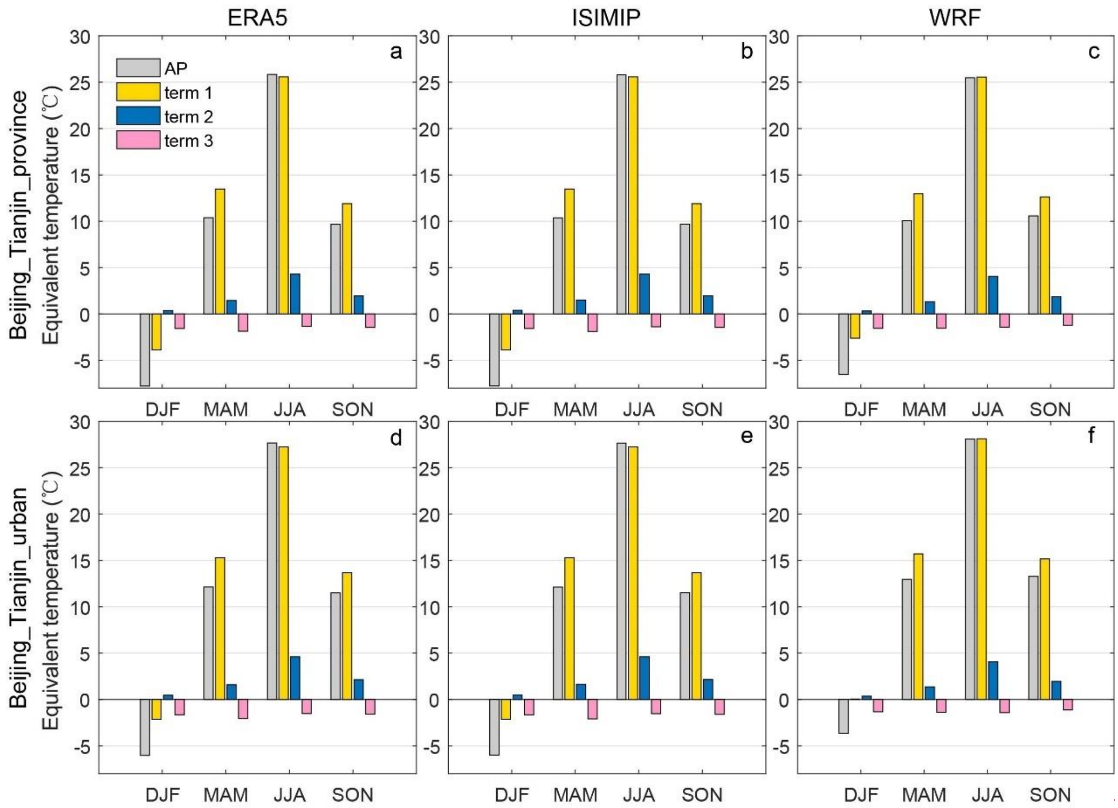

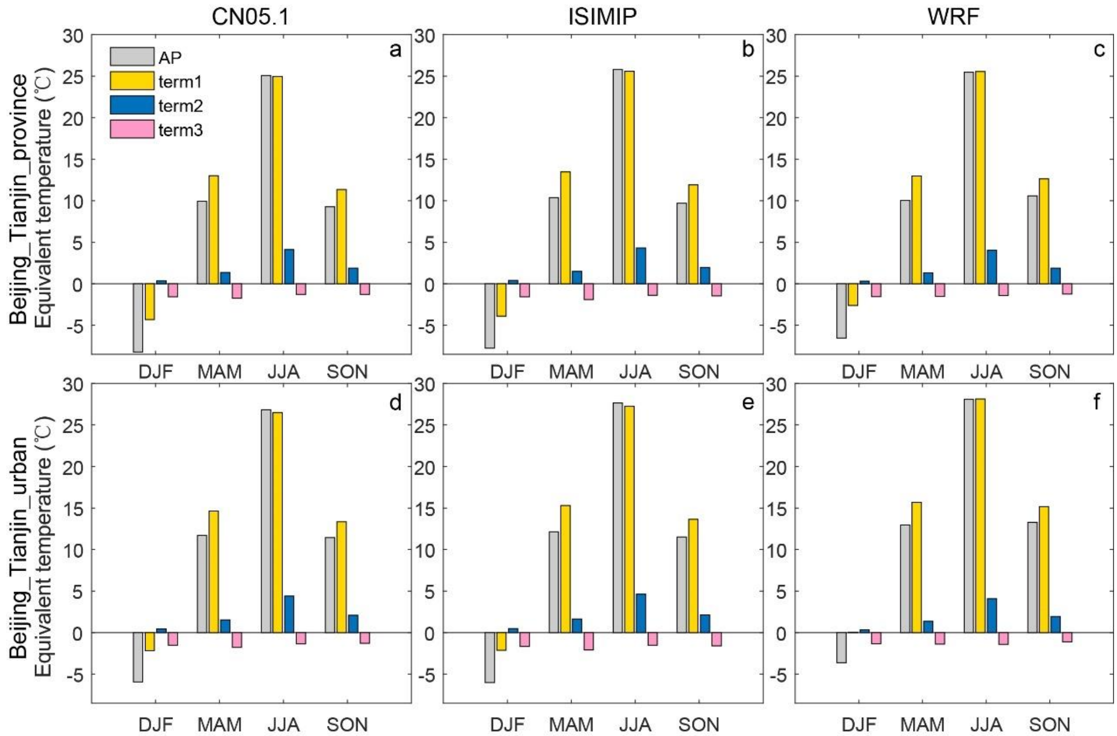

Figure ~~2~~3. Seasonal averaged AP and equivalent temperature of each term in equation 1 for Beijing-

Tianjin province **(a-c)** and Beijing-Tianjin urban areas **(d-f)** during 2008-2017 from ~~ERA5~~CN05.1 **(a, d)**, 4-model ensemble mean after ISIMIP **(b, e)** and ensemble mean after WRF **(c, f)**. Term 1 is 1.04T, term 2 is 2P and term 3 is -0.65W.

Figure ~~2~~3 shows the seasonal averaged AP and equivalent temperatures caused by temperature, relative humidity and wind speed in Beijing-Tianjin province and Beijing-Tianjin urban areas during 2008-2017. According to the ~~ERA5~~CN05.1 results (Fig. ~~2a~~3a, ~~2d~~3d), AP and the separate 3 terms show similar seasonal patterns over the whole province and just the urban areas. Vapor pressure is higher in summer and wind speed is higher in spring. AP is lower than 2 m temperature in all seasons except summer, and especially lower in winter. AP, temperature, vapor pressure and wind speed are all higher in urban areas than in the surrounding rural region in any season. The ISIMIP results (Fig. ~~2b~~3b, ~~2e~~3e), by design, perfectly reproduce the ~~ERA5~~ CN05.1 seasonal characteristics of AP, temperature, vapor pressure and wind speed. WRF shows a similar pattern with that from ~~ERA5~~CN05.1, but for the Beijing-Tianjin province, WRF overestimates both 2 m temperature and AP in winter by 2.1°C and by ~~2.4~~1.7°C respectively relative to ~~ERA5~~ CN05.1 (Fig. ~~2c~~3c). In the Beijing-Tianjin urban areas, WRF overestimates the temperature and AP relative to ~~ERA5~~ CN05.1 in all seasons, especially in winter (Fig. ~~2f~~3f).

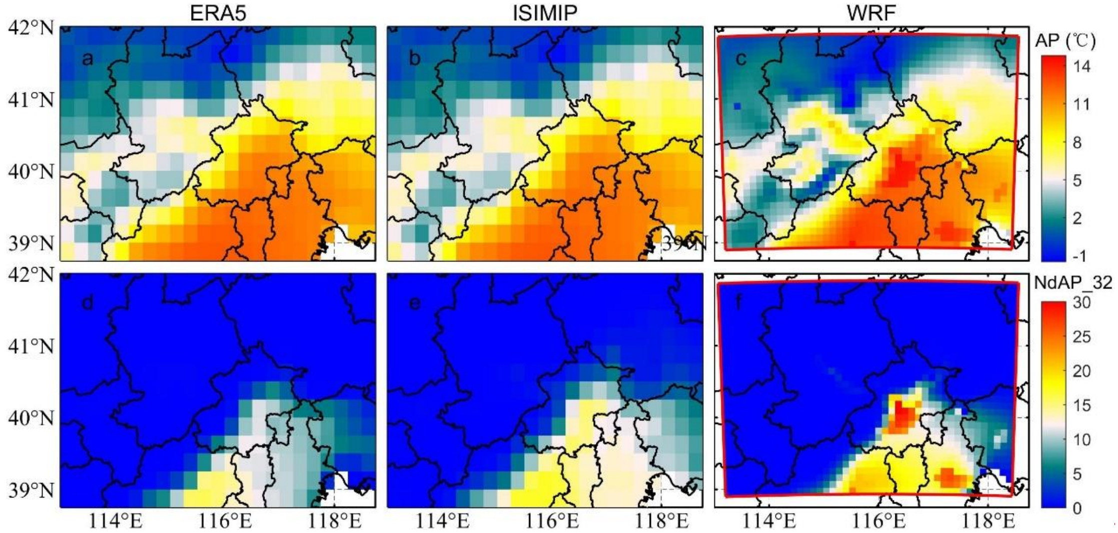

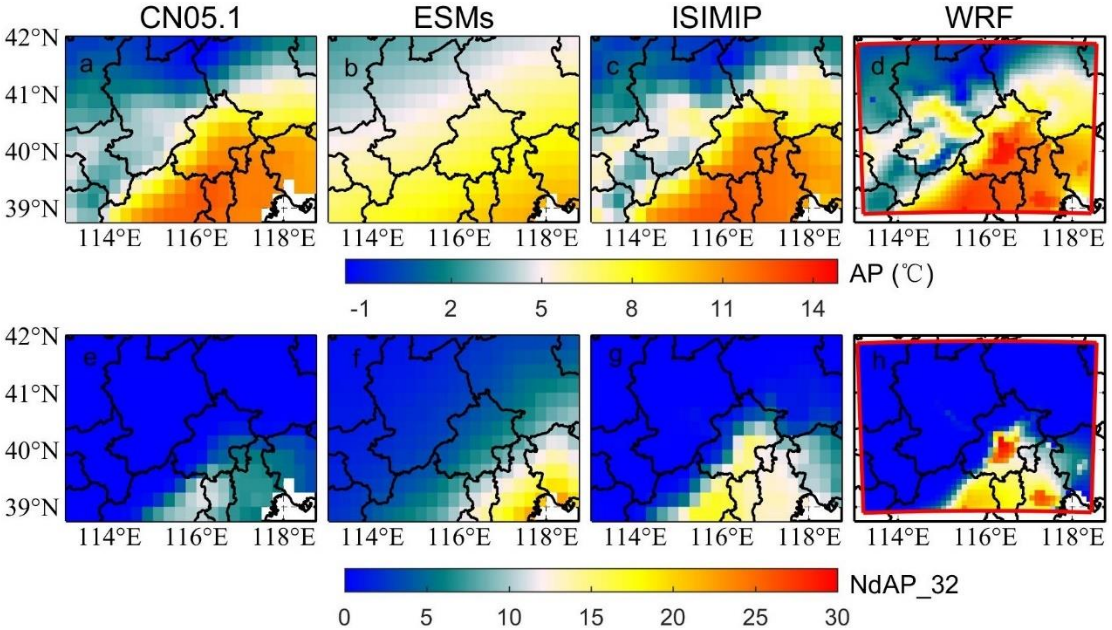

Figure ~~3~~4. Top row: the spatial distribution of mean apparent temperature from ~~ERA5~~ CN05.1 **(a),** raw ESMs ensemble mean after bilinear interpolation **(b),** 4-model ensemble mean after ISIMIP **(~~b~~c)** and ensemble mean after WRF **(~~c~~d)** during 2008-2017. Bottom row: the spatial distribution of annual mean number of days with AP > 32℃ from ~~ERA5~~ CN05.1 **(~~e~~d)**, ESMs **(f)**, ISIMIP **(e)** and WRF **(f)** during 2008-2017. Fig. ~~S1~~ S4 and Fig. ~~S2~~ S5 show the pattern of AP and NdAP_32 for the individual ESM.

We compare the simulations of mean apparent temperature and NdAP_32 from both WRF dynamical downscaling with QDM and from ISIMIP statistical downscaling during 2008-2017 in Fig. ~~3~~4. Both WRF with QDM and ISIMIP methods produce a pattern of apparent temperature which is close to that from ~~ERA5~~CN05.1. While the raw AP from ESMs is overestimated in Zhangjiakou high mountains and underestimated in the southern plain, and shares a similar pattern with temperature from ESMs (Wang et al., 2022). The raw ESM outputs were improved after dynamical and statistical downscaling. The average annual AP from ISIMIP (9.6-9.7°C) is ~~almost the same as~~0.5°C higher than that from ~~ERA5~~ CN05.1 (9.1°C) over the Beijing-Tianjin province for all ESMs (Table 1). While WRF produces warmer apparent temperatures in the city centers of Beijing and Tianjin and lower ones in the high Zhangjiakou mountains than recorded in the lower resolution ~~ERA5~~ CN05.1 observations. There are also differences between different models after WRF downscaling. For example, apparent temperatures from the two MIROC models ~~from~~ downscaled by WRF are the warmest. In contrast AP from all 4 ESMs after ISIMIP shows very similar patterns (Fig. ~~S1~~S4).

ESMs tend to overestimate the number of days with AP>32℃ in southeastern Beijing and the whole Tianjin province. Both ISIMIP and WRF appear to overestimate the NdAP_32 in Beijing urban areas and the southerly lowland areas although NdAP_32 is close to zero ~~for all methods~~ in the colder rural areas at relatively high altitude for both downscaling methods. ~~While s~~Some of these differences may be due to the WRF simulations being at finer resolution than the 0.25°× 0.25° CN05.1, leading to higher probabilities of high AP in urban areas (Fig. 5d). ISIMIP results also show slight overestimations, especially in the tails of the distribution (AP>30℃) for urban areas (Fig. 5c).~~0.25°×0.25° resolution ERA5, which is coarser than the 10 km WRF simulation, it probably does not account for the broad overestimate across most the North China Plain that is within the WRF and ISIMIP domains.~~ ~~ERA5~~ CN05.1 gives about ~~10~~ 5 NdAP_32 per year in southern Beijing and Tianjin, but there are nearly 15 NdAP_32 from ISIMIP, and over 20 ~~NaAP~~NdAP_32 per year from WRF downscaling in the Beijing-Tianjin urban areas during 2008-2017. NdAP_32 from WRF and ISIMIP downscaling of all ESM is overestimated relative to ~~ERA5~~CN05.1. But there are ~~curious~~ differences in ESM under the two downscalings: with ISIMIP, HadGEM2-ES and BNU-ESM have more NdAP_32 than the two MIROC models, while the reverse occurs with WRF (Fig. ~~S2~~S5).

Table 1. The annual mean apparent temperature and population weighted NdAP_32 in Beijing-Tianjin province and Beijing-Tianjin urban areas (Fig. 1b) from ~~ERA5~~CN05.1, ISIMIP and WRF during 2008-2017.

Data Sources	AP (℃)				NdAP_32 (day yr^{-1})	
	Provinces		Urban		Population weighted for province (Fig. 1c, 1d)	
	WRF	ISIMIP	WRF	ISIMIP	WRF	ISIMIP
MIROC-ESM	10.5	9.6	13.6	11.4	22.2	10.1
MIROC-ESM-CHEM	10.5	9.6	13.6	11.4	21.9	11.0
HadGEM2-ES	9.5	9.6	12.0	11.4	12.3	11.1
BNU-ESM	9.4	9.7	11.8	11.5	10.2	12.7
~~ERA5~~CN05.1	9.~~6~~1		11.41		~~7.7~~2.4	

The Taylor diagram of the daily mean apparent temperature in Beijing-Tianjin province and Beijing-Tianjin urban areas from 2008-2017 for the 4 ESMs shows that ~~all models under both downscaling methods have~~ correlation coefficients between ESMs and

CN05.1 are greater than 0.85 under both downscaling methods. ~~with ERA5 > 0.85.~~ Although there are differences between ESMs, the performance of WRF, with higher correlation coefficient and smaller SD (standard deviation) and RMSD (root mean standard deviation), is usually superior to ISIMIP~~Although AP over the both whole Beijing-Tianjin province and the urban areas are overestimated by WRF, it performs slightly better than ISIMIP on the Taylor plot relative to ERA5~~ (Fig. ~~S3~~S6). Taking the Beijing-Tianjin urban areas as an example (Fig. S6b), ~~Under~~ under the ISIMIP method, MIROC-ESM, MIROC-ESM-CHEM and HadGEM2-ES have the same correlation coefficient (0.92) and RMSD (5.4℃) with the CN05.1, ~~show little differences in correlation or errors~~ while ~~the performance of~~ BNU-ESM has lower correlation coefficient (0.88) and higher RMSD (7.0℃).~~is slightly worse.~~ Under WRF simulations, MIROC-ESM and MIROC-ESM-CHEM have larger correlation coefficients and smaller ~~errors~~ RMSD with CN05.1 than HadGEM2-ES and BNU-ESM.

Figure ~~4~~ 5 shows the probability density functions (pdf) of daily AP from the four ESMs under ISIMIP and WRF in Beijing-Tianjin province and Beijing-Tianjin urban areas during 2008-2017. ISIMIP overestimates the probability of extreme cold AP relative to ~~ERA5~~ CN05.1 (especially BNU-ESM), although all ESM reproduce the ~~ERA5~~ CN05.1 pdf well at high AP. WRF can reproduce the ~~ERA5~~ CN05.1 distribution of AP better than ISIMIP, but high AP is overestimated relative to ~~ERA5~~ CN05.1 and the urban areas perform less well than the whole Beijing-Tianjin province. In urban areas all ESMs driving WRF tend to underestimate the probability of lower AP and to overestimate the probability of higher AP, especially the two MIROC models (Fig. ~~4d~~5d). Fig. ~~S4~~ S7 displays the annual cycle of monthly AP, with ISIMIP proving excellent by design, at reproducing the monthly AP. While under WRF downscaling AP shows more across model differences, especially during summer and with greater spread for the urban areas.

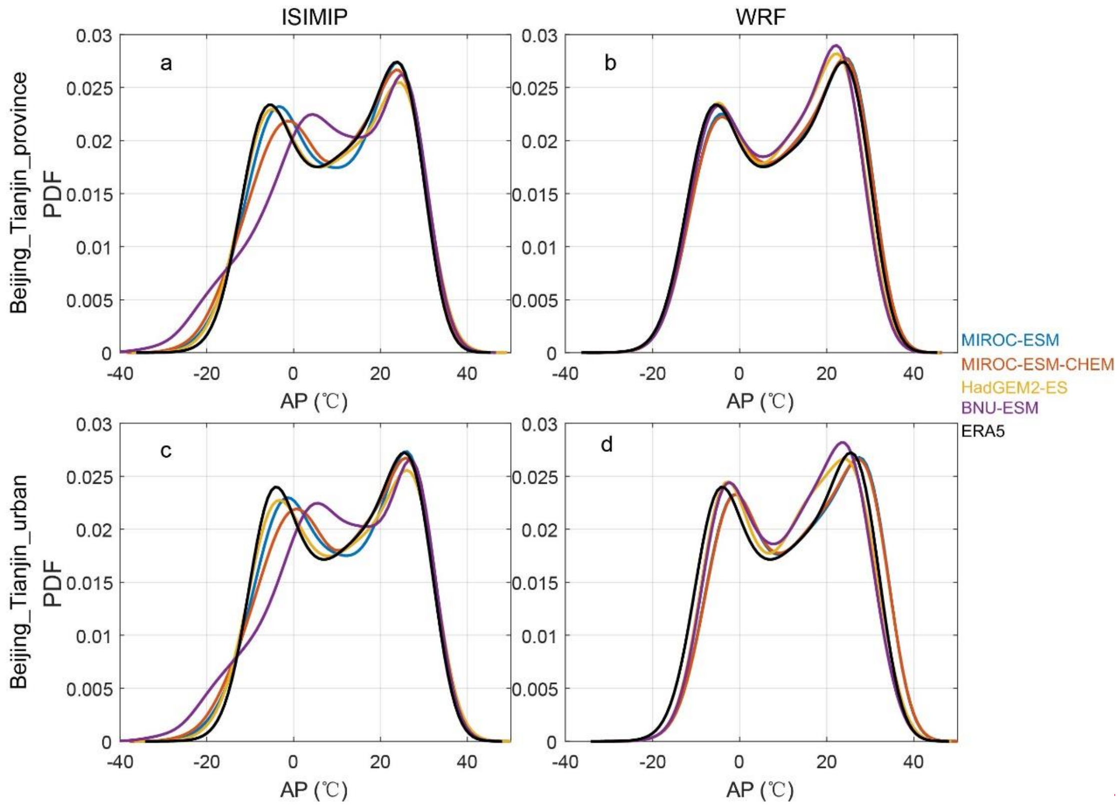

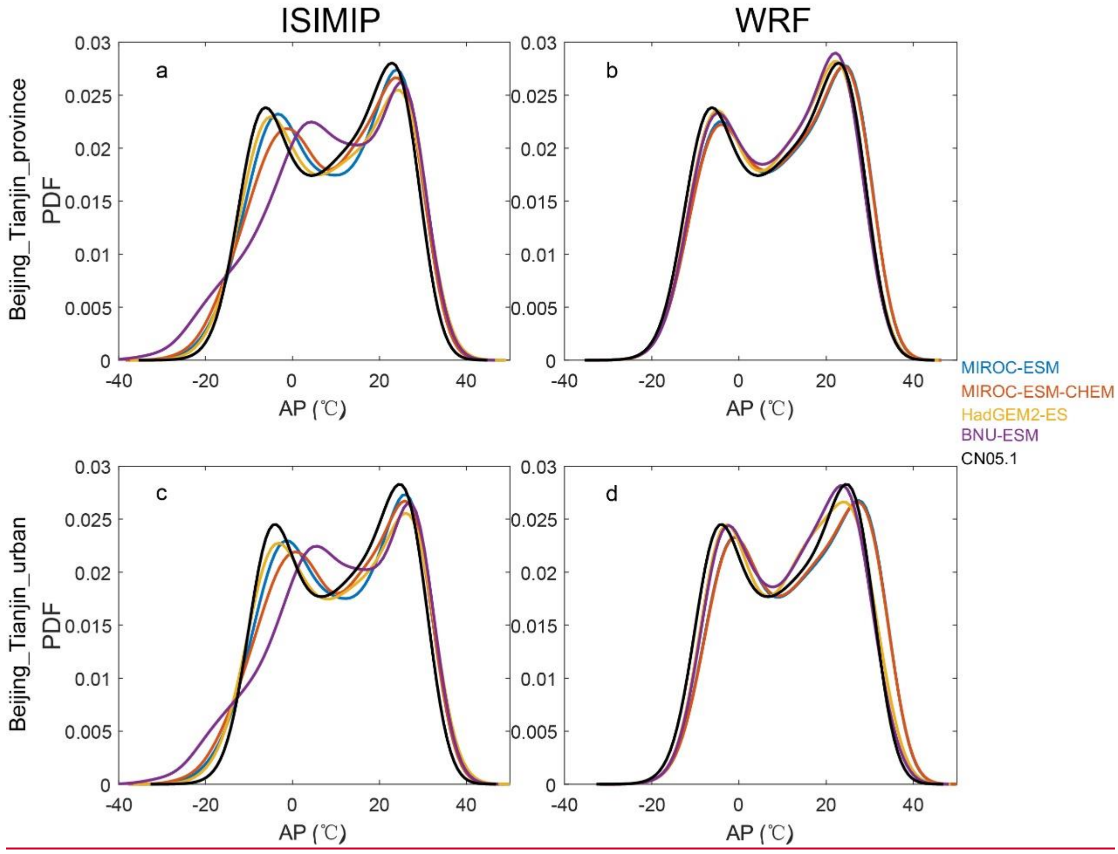

Figure 45. The probability density function (pdf) for daily apparent temperature under ISIMIP **(a, c)** and WRF **(b, d)** results in Beijing-Tianjin province **(a, b)** and Beijing-Tianjin urban areas **(c, d)** during 2008-2017.

3.2 2060s apparent temperatures

3.2.1 Changes of apparent temperature

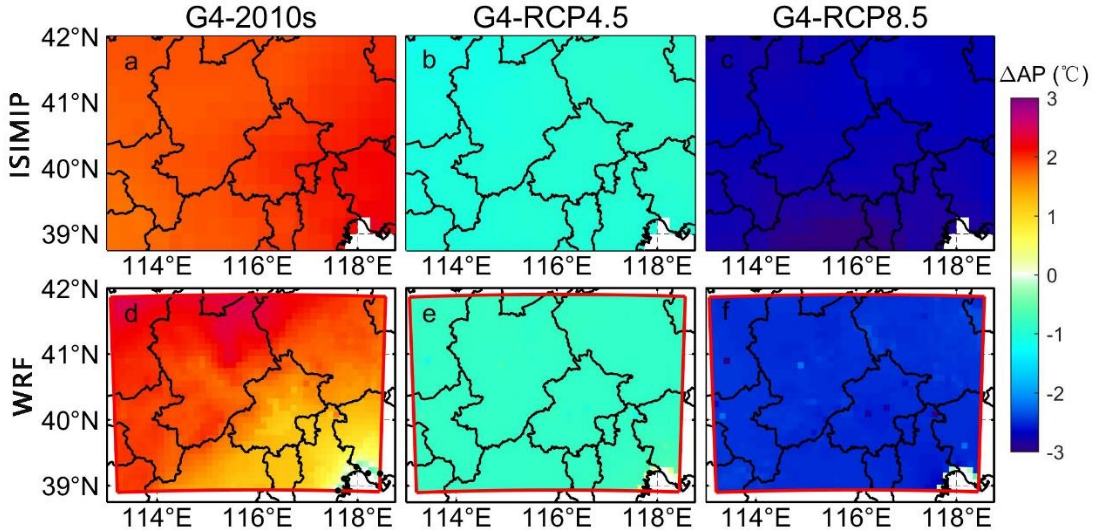

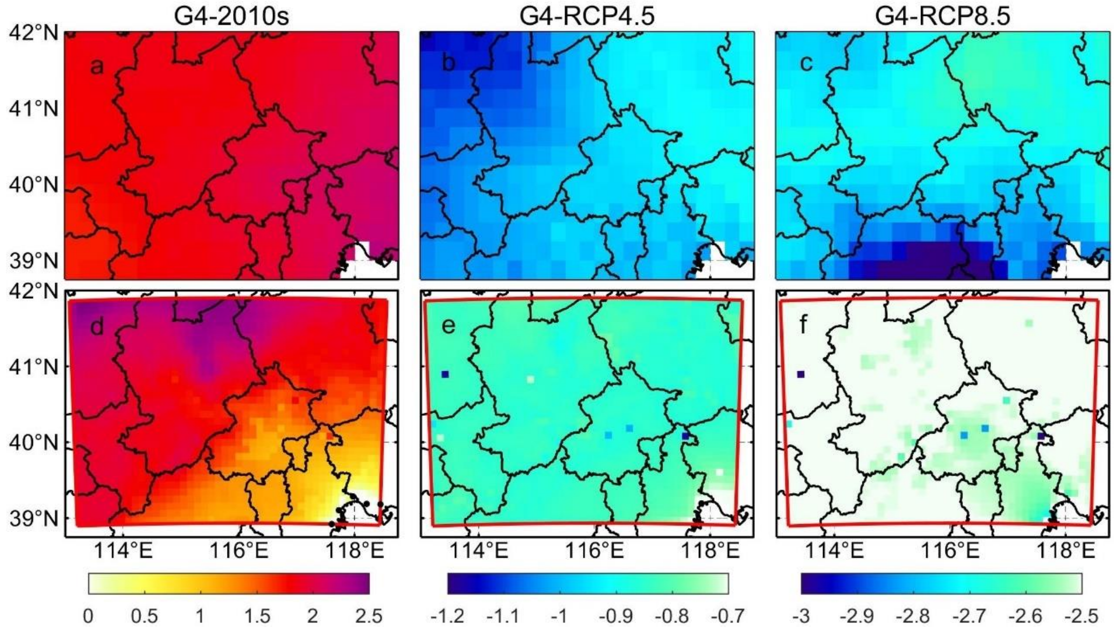

Figure 6~~5~~. Spatial pattern of ensemble mean apparent temperature difference (℃) under different scenarios over 2060-2069: G4-2010s (left column), G4-RCP4.5 (middle column) and G4-RCP8.5 (right column) based on ISIMIP and WRF methods. 2010s refers to the 2008-2017 period. Stippling indicates grid points where differences or changes are not significant at the ~~9~~5% level according to the Wilcoxon signed rank test.

Figure ~~5~~ 6 shows the ISIMIP and WRF ensemble mean changes in the annual mean AP under G4 during 2060-2069 relative to the past and the two future RCP scenarios. ISIMIP-downscaled AP (Fig. ~~5a~~6a-~~5c~~6c) shows significant anomalies ($p<0.05$), with whole domain rises of 2.0 °C in G4-2010s, and falls of 1.0 °C and 2.8 °C in G4-RCP4.5

and G4-RCP8.5 respectively~~ across the whole domain, even for the relatively small differences in G4-RCP4.5~~. In WRF results, AP under G4 is about 1-2 °C warmer than that under 2010s, 0.8 °C and 2.5 °C colder than that under RCP4.5 and RCP8.5 over the whole domain.~~There are no models with obvious regional differences in AP anomalies (Fig. S6). G4 is about 2°C warmer than the 2008-2017 period and about 1°C colder than RCP4.5 and 3°C colder than RCP8.5. WRF downscaling (Fig. 5d-5f) anomalies are similar but the warming under G4 relative to the 2010s is smaller and the coolings relative to both RCP scenarios are a little smaller than those under ISIMIP.~~ Individual ESM ~~driven~~ results downscaled by ISIMIP ~~results~~ and WRF are in Fig. ~~S6~~ S9 and ~~WRF results in~~ Fig. ~~S7~~S10. For both ISIMIP and WRF downscaling results, the two MIROC models show stronger warming than the other two models between G4 and the 2010s. WRF-downscaled AP driven by HadGEM2-ES exhibits the strongest cooling, with decreases of 1.7 °C between G4 and RCP4.5 and falls of 3.0 °C between G4 and RCP8.5. Although different ESMs show different changes in AP between G4 and other scenarios, changes in AP are almost the same everywhere for a given ESM in the ISIMIP results (Fig. S9). WRF-downscaled AP anomalies driven by two MIROC models are larger in the Zhangjiakou mountains and smaller in the Beijing urban areas and Tianjin city between G4 and 2010s (Fig. S10). ~~(> 1.5°C for G4-RCP4.5 and 3°C for G4-RCP4.5).~~ Changes in AP from ISIMIP results, whether across whole province or just the urban areas, are statistically identical given scenarios~~AP changes, whether across all province or just urban areas, are essentially the same~~ (Table 2), which is consistent with patterns in figure ~~5~~6. AP under G4 is 0.8 °C (1.0 °C) and 2.6 °C (2.8 °C) colder than that under RCP4.5 and RCP8.5 in Beijing-Tianjin urban areas from ISIMIP (WRF) results. The warming between G4 and 2010s in urban areas is 1.0 °C in WRF results, while that is 2.0 °C in ISIMIP results (Table 2).~~The ensemble mean differences in AP between G4 and RCP scenarios calculated both using ISIMIP and WRF downscaling are small, however ensemble mean AP differences between G4 and the 2010s over urban areas are 1.0°C under WRF and 2.0°C, under ISIMIP.~~

Table 2. Difference of apparent temperature between the G4 and other scenarios for the Beijing-Tianjin province and Beijing-Tianjin urban areas as defined in Fig. 1b during 2060-2069. Bold indicates the differences or changes are significant at the 5% level according to the Wilcoxon signed rank test. (Units: °C)

Model	G4-2010s				G4-RCP4.5				G4-RCP8.5			
	WRF		ISIMIP		WRF		ISIMIP		WRF		ISIMIP	
	Urban	Province	Urban	Province	Urban	Province	Urban	Province	Urban	Province	Urban	Province
MIROC-ESM	**0.9**	**1.5**	**2.2**	**2.2**	**-0.5**	**-0.4**	**-0.9**	**-0.9**	**-2.3**	**-2.1**	**-2.8**	**-2.7**
MIROC-ESM-CHEM	**0.9**	**1.5**	**2.9**	**2.8**	**-0.4**	**-0.4**	-0.1	-0.1	**-2.0**	**-2.0**	**-2.1**	**-2.1**
HadGEM2-ES	**1.1**	**1.0**	**1.8**	**1.7**	**-1.6**	**-1.6**	**-1.6**	**-1.6**	**-3.1**	**-3.1**	**-3.3**	**-3.3**
BNU-ESM	**1.2**	**1.1**	**1.2**	**1.3**	**-0.8**	**-0.8**	**-1.3**	**-1.3**	**-2.8**	**-2.7**	**-2.9**	**-2.9**
Ensemble	**1.0**	**1.3**	**2.0**	**2.0**	**-0.8**	**-0.8**	**-1.0**	**-1.0**	**-2.6**	**-2.5**	**-2.8**	**-2.8**

3.2.2 Contributing factors to changes in AP

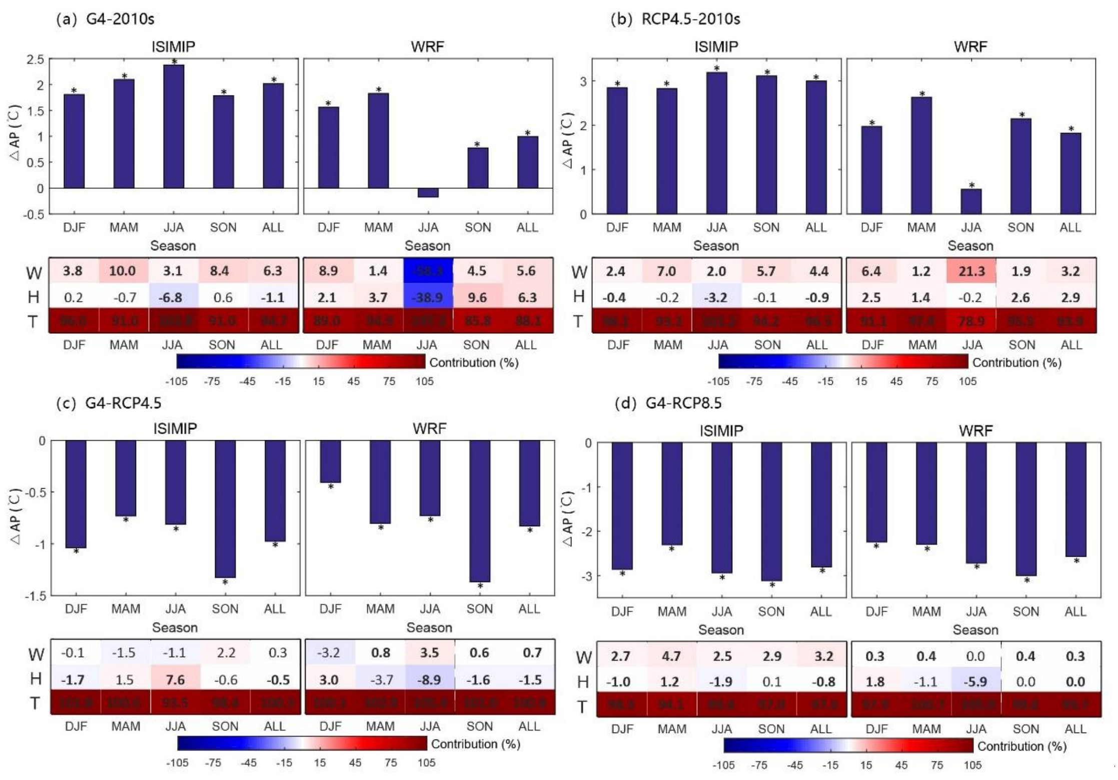

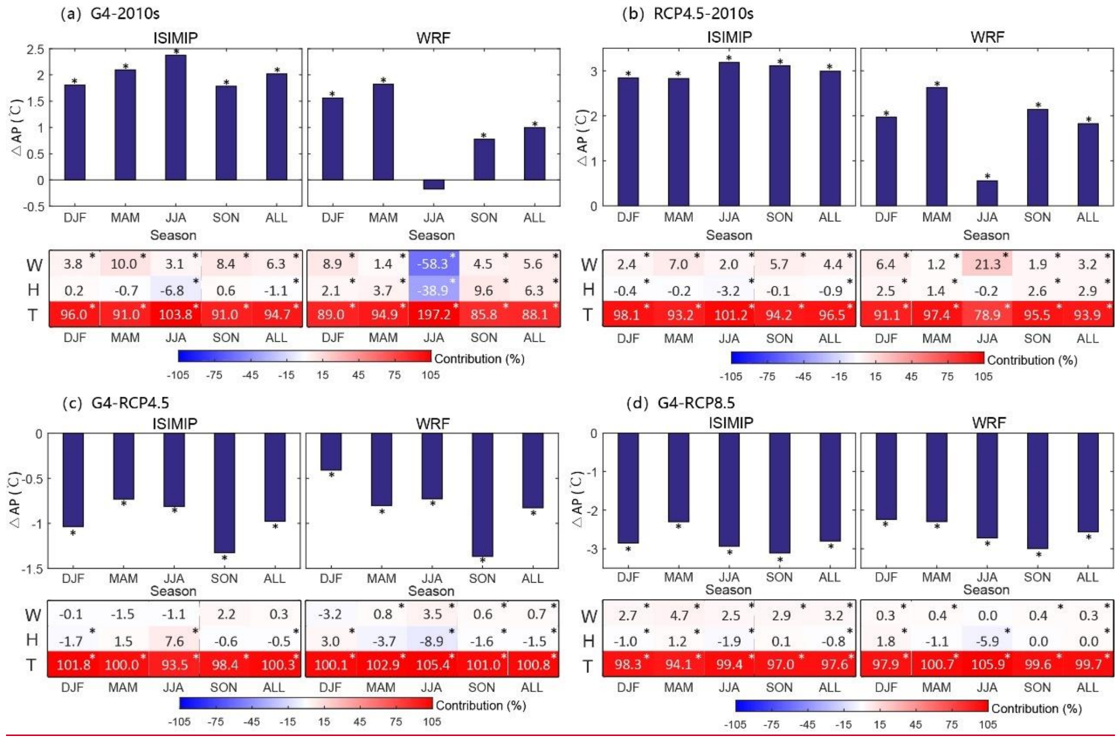

Figure ~~6~~7. The seasonal changes of AP (ΔAP) and the seasonal contribution of climatic factors to ΔAP for Beijing and Tianjin urban areas under ISIMIP and WRF between G4 and 2010s **(a)**, G4 and 2010s **(b)**, G4 and RCP4.5 **(c)** and G4 and RCP8.5 **(d)** in the 2060s based on ensemble mean results. Colors and numbers in each cell correspond to color bar, ~~Bold tabulated numbers~~ and "*" above the columns and in the cells indicate differences are significant at the ~~9~~5% significant level under the Wilcoxon test.

Figure 7 shows the ISIMIP and WRF ensemble mean changes in the annual mean AP anomalies G4 during 2060-2069 relative to the past and the two future RCP scenarios. ISIMIP-downscaled AP (Fig. 7a-7c) shows significant anomalies ($p<0.05$) across the whole domain, even for the relatively small differences in G4-RCP4.5. ΔAP by WRF is lower than that by ISIMIP. Between G4 and 2010s, AP are projected to have increases of 1.8 (1.6), 2.1 (1.8), 2.4 (-0.2), 1.8 (0.8) °C from winter to autumn in ISIMIP (WRF) results. In ISIMIP results, the contribution of temperature ranges from 91%-104%, and the contribution of wind speed ranges from 3%-10% in all seasons, while the contribution of humidity is negative or insignificant (Fig. 7a). However, the contribution of humidity is positive in WRF results (Fig. 7a). Between RCP4.5 and 2010s, annual mean AP is projected to increase by 3.0 °C and 1.8 °C in ISIMIP and WRF results respectively, which is higher than that between G4 and 2010s. The increase of temperature and decrease of wind speed have a significant impact on the annual average ΔAP contributed 97% (94%) and 4% (3%) in ISIMIP (WRF) results. The contributions of changes in humidity are significantly positive under G4 and RCP4.5 in WRF results, while it is the opposite in the ISIMIP results (Fig. 7a-7b).

Relative to RCP4.5 in the 2060s, AP is projected to decrease by 1.0 (0.4), 0.7 (0.8), 0.8 (0.7), and 1.3 (1.4) °C from winter to autumn under G4 in ISIMIP (WRF) results (Fig. 7c). In summer, the contribution from changes in temperature and humidity are 94% (105%) and 8% (-9%) in ISIMIP (WRF) results, respectively. There are insignificant contributions from wind speed under ISIMIP results, but a significant slight positive contribution (0.7%-4%) under WRF results (Fig. 7c). The annual mean AP under G4 is 2.8 (2.6) °C lower than that under RCP8.5 in ISIMIP (WRF) result. In this case, the contribution of changes in wind on ΔAP ranges from 3%-5% by ISIMIP, while it is close to 0 by WRF. As expected, ΔAP is mainly determined by the changes in temperature, with contributions usually above 90% between different scenarios.
~~We show the seasonal contribution of temperature, humidity and wind to differences in AP between G4, the 2010s, RCP4.5 and RCP8.5 from ISIMIP and WRF downscaling over Beijing-Tianjin urban areas in Fig. 6. Undoubtedly, temperature makes the biggest contribution to ΔAP between different scenarios, and ΔAP is smaller under WRF than under ISIMIP. The projected differences in scenario temperatures explain more than 90% of the ΔAP differences. There are striking differences between WRF and ISIMIP in the seasonal contribution of humidity to ΔAP for both G4 and RCP4.5 relative to the 2010s (Fig. 6a, 6b). Under WRF, summer differences in humidity makes a negative contribution to ΔAP for G4 while under RCP4.5 humidity makes only a slightly negative but non-significant contribution, but the summer ΔAP is much lower than in other seasons. Wind increases ΔAP under both G4 and RCP4.5 relative to the 2010s. Fig. 6c and 6d show that ΔAP under G4 compared with RCP4.5 and RCP8.5 is significantly affected by humidity in summer. The negative contributions from humidity under WRF amount to 6-9%, but under ISIMIP the contributions are much smaller, and even acts to reduce differences in ΔAP between G4 and RCP4.5. Changes in wind are insignificant for ΔAP between G4 and RCP4.5 under ISIMIP, but with WRF changes in wind are generally significant and amount to over 3% in summer. In contrast, the seasonal contribution of wind is about 2.5-4.7% under ISIMIP to differences~~

~~between G4 and RCP8.5 but close to 0 under WRF.~~

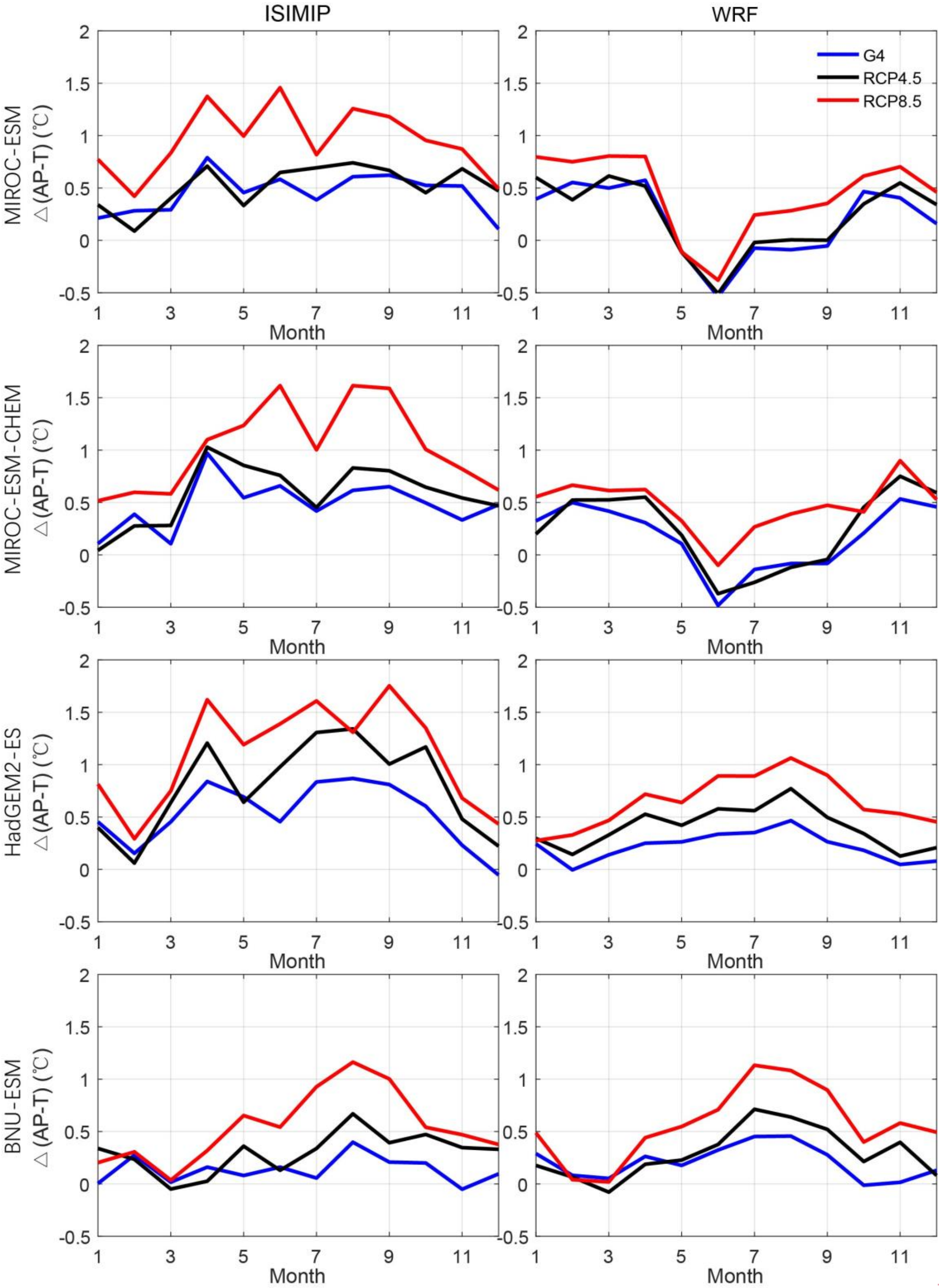

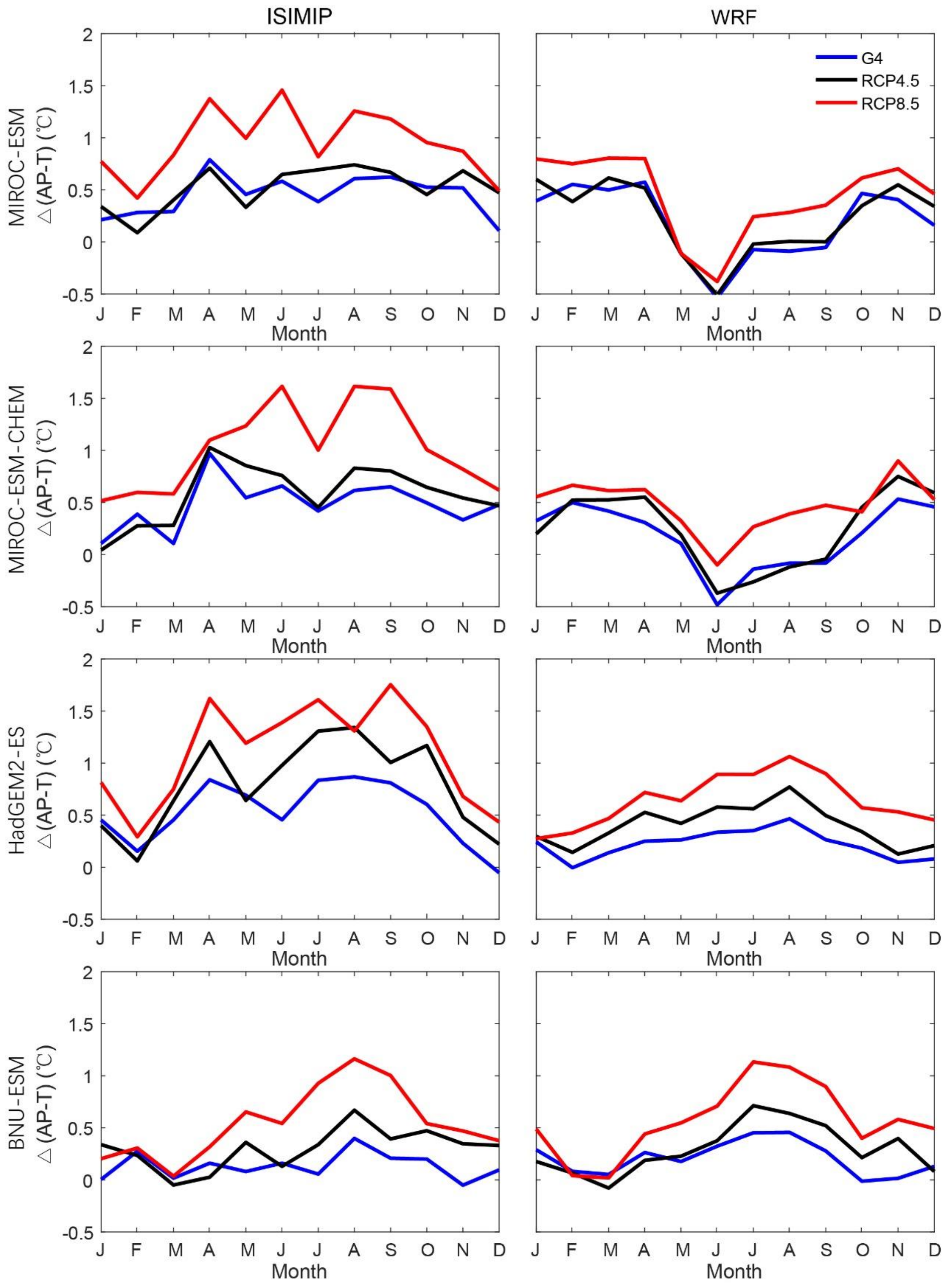

Figure ~~7~~8. The change of apparent temperature based on air temperature under three scenarios (G4, RCP4.5 and RCP8.5) in four ESMs under ISIMIP (left column) and WRF (right column) for urban areas relative to the 2010s.

A useful measure of heat impacts that may be missed if considering only at air temperatures is the seasonality of the differences between AP and air temperature (Δ(AP-T); Fig. ~~7~~8). The four model ensemble annual mean Δ(AP-T) under ISIMIP is projected to rise by 0.4℃, 0.5℃ and 0.9℃ under G4, RCP4.5 and RCP8.5, relative to the 2010s. Under WRF, Δ(AP-T) is much smaller than under ISIMIP but still rising faster than air temperatures: by 0.2℃, 0.3℃ and 0.5℃ under G4, RCP4.5 and RCP8.5 relative to the 2010s, respectively. In general, the largest anomalies in Δ(AP-T) are in summer under both WRF and ISMIP downscaling, but the two MIROC models under WRF have small or even negative Δ(AP-T) in summer with WRF.

3.2.~~2~~ 3 Changes of the number of days with AP>32℃

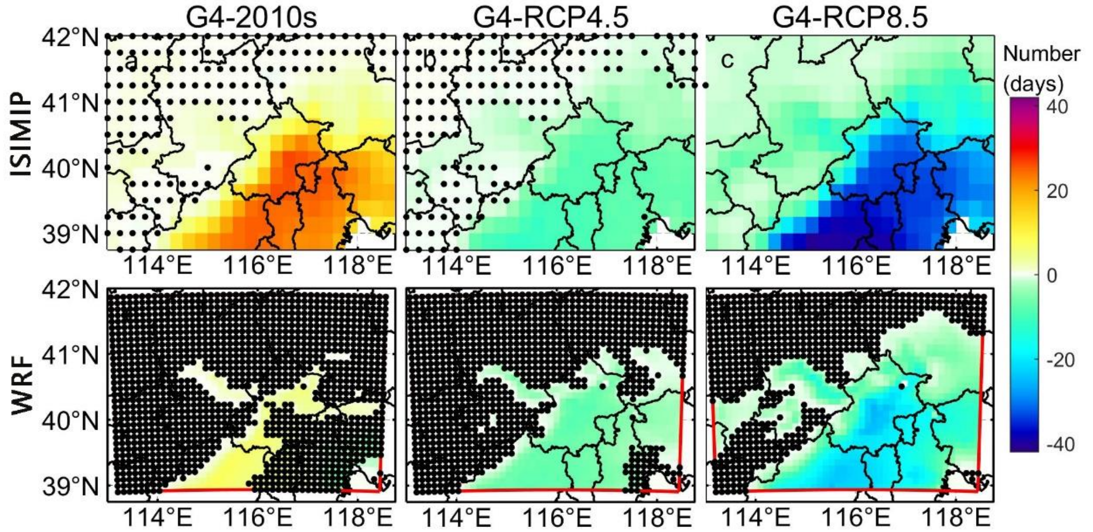

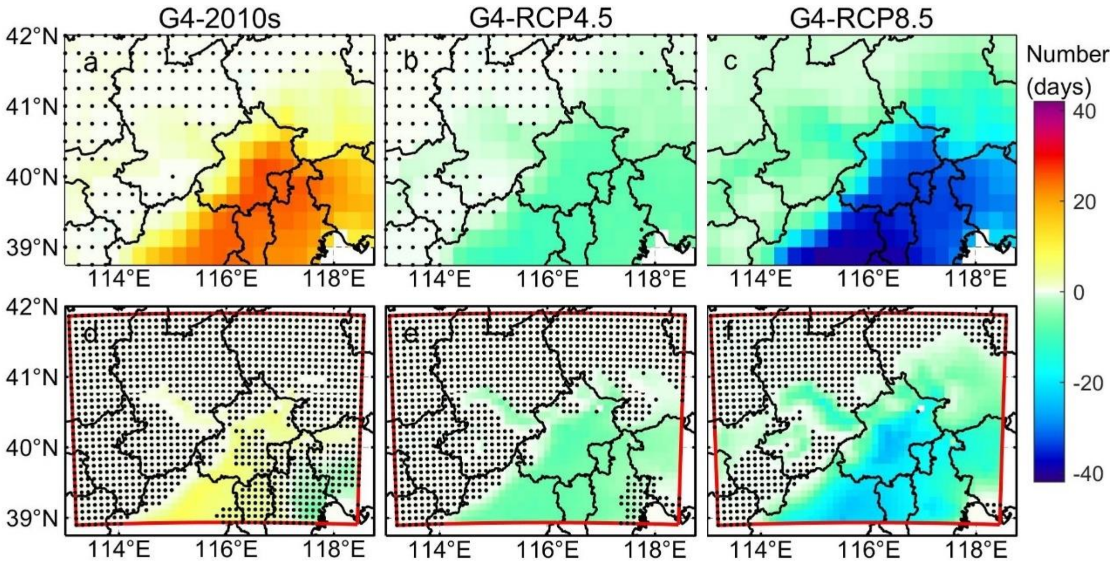

Figure 9~~8~~. Ensemble mean differences in annual number of days with AP > 32℃ (NdAP_32) between scenarios for 2060-2069: G4-2010s (left column), G4-RCP4.5 (second column) and G4-RCP8.5 (right column) based on ISIMIP method and WRF. 2010s means the results simulated during 2008-2017. Stippling indicates grid points where differences or changes are not significant at the 5% level according to the Wilcoxon signed rank test. Corresponding ISIMIP results for each ESM are in Fig. ~~S8~~S11, and WRF results in Fig. ~~S9~~S12.

The NdAP_32 anomalies in Figure ~~8~~ 9 show that ISIMIP projects an increase of about

20 days per year with AP>32 °C for the southeast of Beijing province and 10 days in the western areas of Beijing under G4 relative to the 2010s. NdAP_32 is about 10 days fewer under G4 than RCP4.5 with no clear spatial differences. G4 has about 35 fewer NdAP_32 days in the southern part of the domain and 20 fewer days in the western domain than the RCP8.5 scenario. In contrast WRF suggests that most areas do not show any significant difference between G4 and the 2010s, while the anomalies relative to RCP4.5 are similar as ISIMIP, ~~although~~ the differences are ~~less~~ insignificant over more area than ISIMIP~~.~~. G4-RCP8.5 anomalies with WRF are ~~less significant and~~ smaller than with ISIMIP, and differences are not significant in the Zhangjiakou high mountains. The urban areas show larger decreases in NdAP_32 than the more rural areas, even in the low altitude plain. Individual ESM show almost no statistically significant differences between G4 and RCP4.5 (Fig. ~~S8~~ S11 and ~~S9~~S12), but the differences seen in Fig. ~~8~~ 9 are significant because of the larger sample size in the significance test. All ESMs with ISIMIP show more NdAP_32 in the urban areas under G4 than the 2010s, while two MIROC models driving WRF show fewer NdAP_32 in Beijing-Tianjin urban areas (Fig. ~~S8~~S11, ~~S9~~S12).

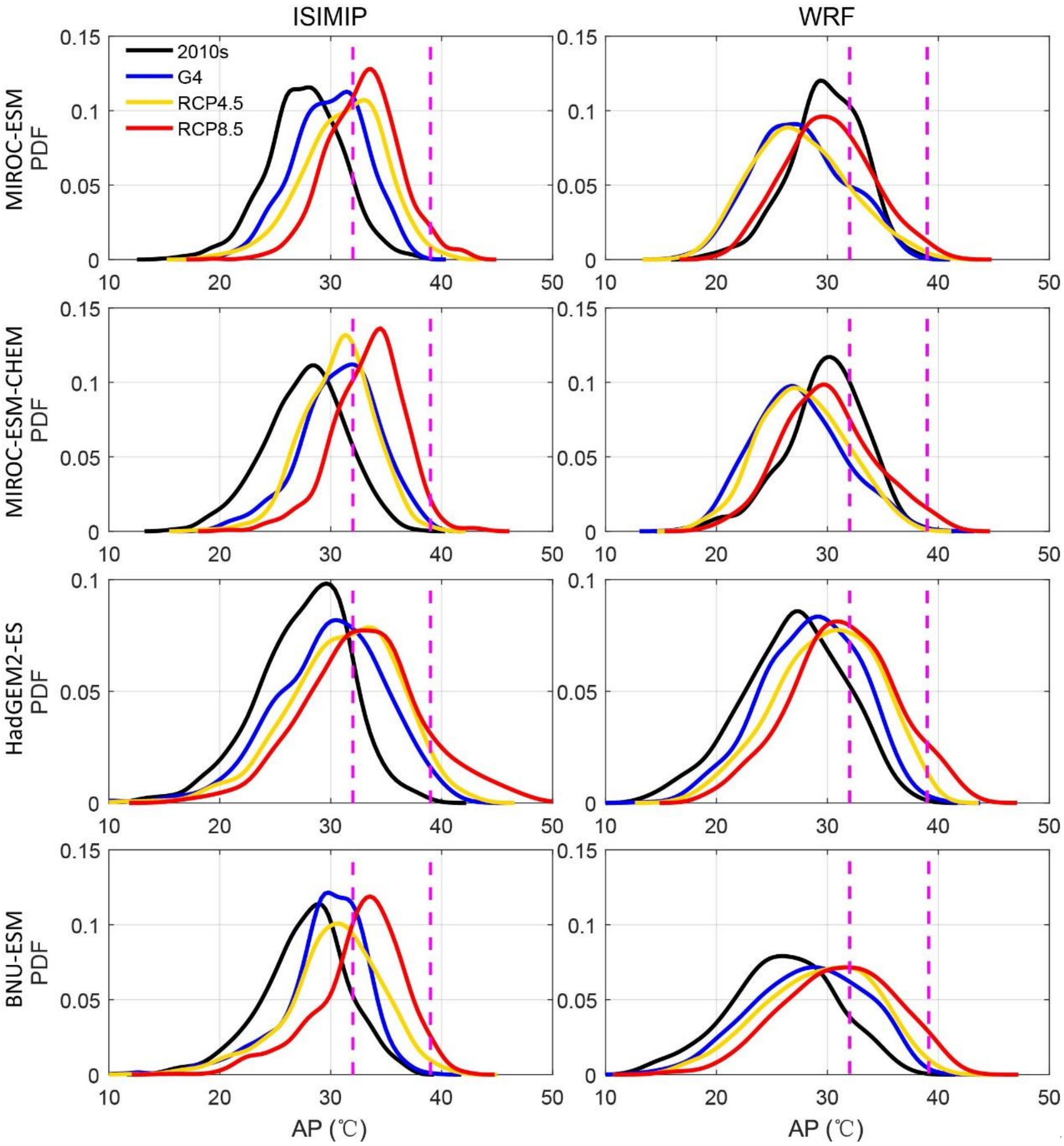
ISIMIP
WRF
2010s
G4
RCP4.5
RCP8.5
MIROC-ESM
PDF
MIROC-ESM-CHEM
PDF
HadGEM2-ES
PDF
BNU-ESM
PDF
AP (℃)
AP (℃)

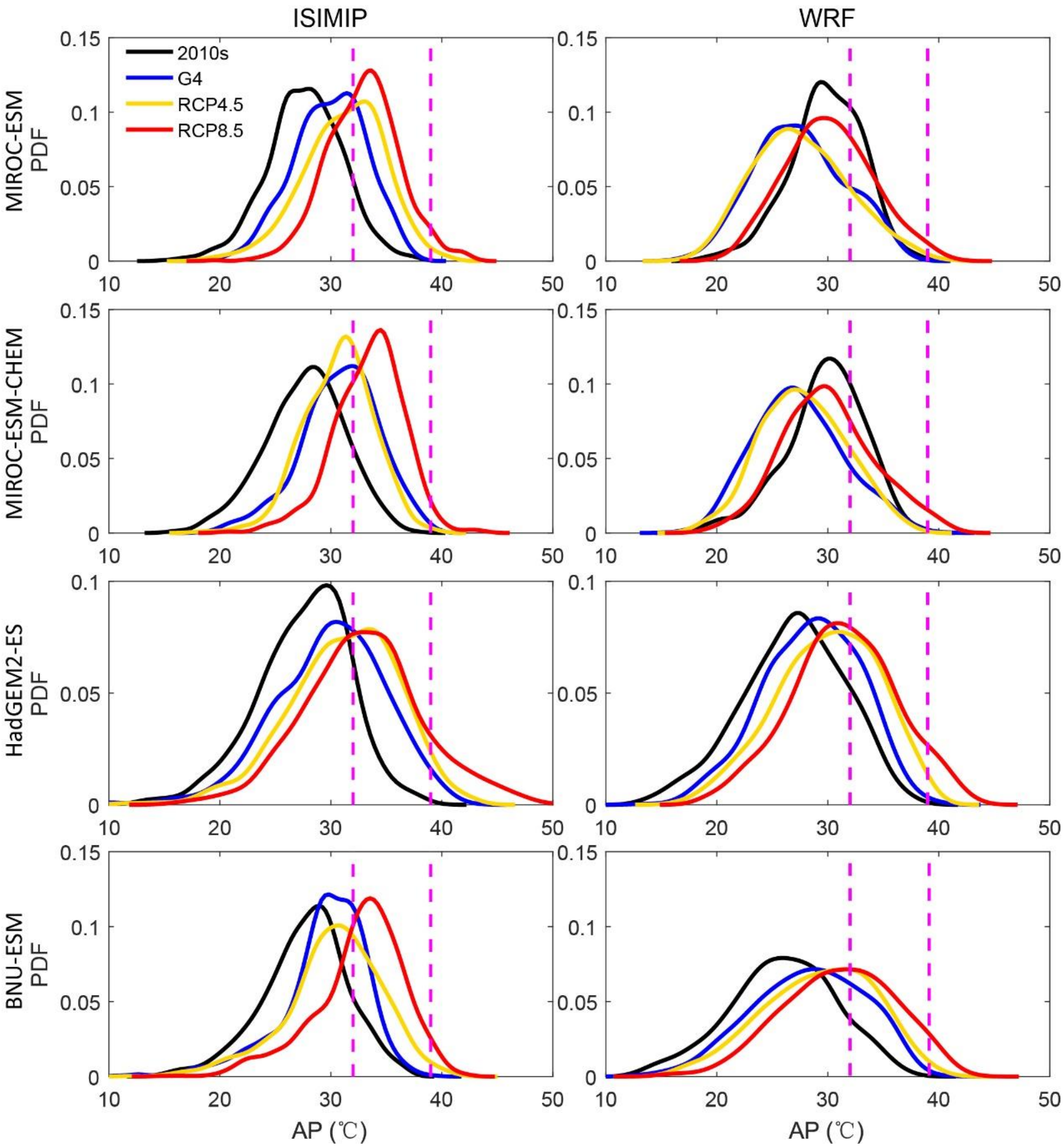

Figure ~~9~~10. Probability density distributions of daily apparent temperature (AP) in summer (JJA) over Beijing-Tianjin urban areas under recent period (2008-2017), and the 2060s under G4, RCP4.5 and RCP8.5 scenarios from ISIMIP and WRF results. The purple dotted lines are at AP of 32℃ and 39℃.

The pdf of daily apparent temperature in summer over Beijing-Tianjin urban areas (Fig. ~~9~~10) shifts rightwards for G4, RCP4.5 and RCP8.5 during the 2060s relative to the 2010s. Figure ~~9~~ 10 shows that by the 2060s, the dangerous threshold of AP>39 is crossed frequently under RCP8.5 with both WRF and ISIMIP downscaling, but for the RCP4.5 and G4 scenarios these events are much rarer. ISIMIP results tend to show higher probability tails (extreme events) than under WRF simulations.

Population weighted NdAP_32 in the 2060s for Beijing-Tianjin province is shown in Table 3. ISIMIP downscaling suggests ensemble mean rises in NdAP_32 of 22.4 days per year under G4 relative to the 2010s, but that G4 has 8.6 and 33.5 days per year fewer than RCP4.5 and RCP8.5, respectively. NdAP_32 from WRF under G4 is reduced by 19.6 days per year relative to RCP8.5, and by 6.3 days relative to RCP4.5 (Table 3).

Table 3. Difference of population weighted NdAP_32 between the G4 and other scenarios for Beijing-Tianjin province (Fig. 1c, 1d) during 2060-2069. Bold indicates the changes are significant at the 5% level according to the Wilcoxon signed rank test. (Units: day y^{-1}).

Beijing-Tianjin province	G4-2010s		G4-RCP4.5		G4-RCP8.5	
	ISIMIP	WRF	ISIMIP	WRF	ISIMIP	WRF
MIROC-ESM	**18.6**	-8.1	-17.0	0.8	**-35.4**	**-13.1**
MIROC-ESM-CHEM	**28.7**	**-10.2**	3.9	-2.2	**-33.7**	**-15.5**
HadGEM2-ES	**25.7**	**9.4**	**-12.5**	**-13.5**	**-24.3**	**-25.3**
BNU-ESM	**16.4**	**13.6**	-8.6	**-10.4**	**-40.5**	**-24.4**
Ensemble	**22.4±2.9**	1.2±6.0	**-8.6±4.5**	**-6.3±3.4**	**-33.5±3.4**	**-19.6±3.1**

3.3 $PM_{2.5}$ in the 2060s

3.3.1 $PM_{2.5}$ scenarios in the 2060s

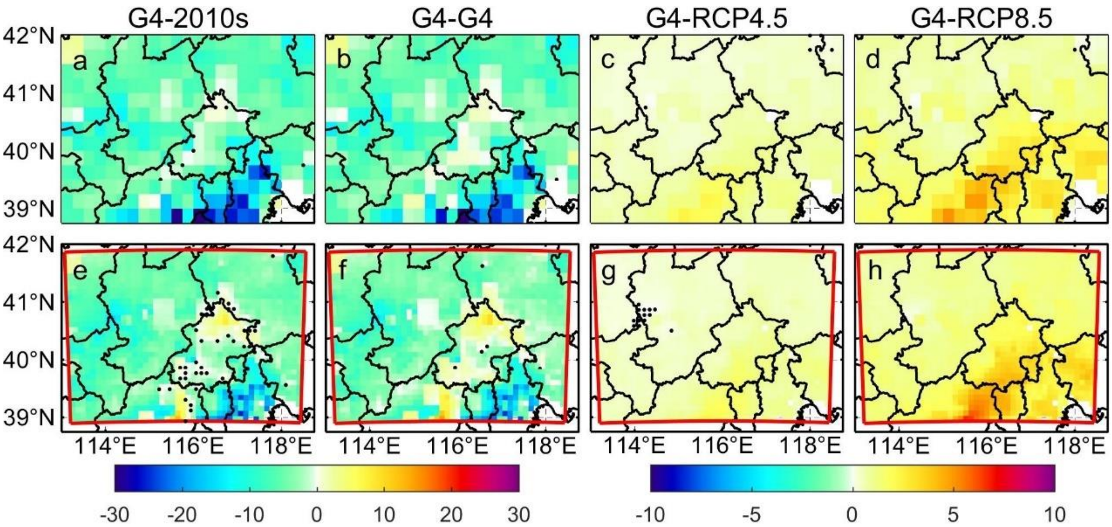

Figure 11. Spatial patterns of ensemble mean $PM_{2.5}$ concentration difference ($\mu g/m^3$) between "mitigation" under G4 in the 2060s and reference **(a, e)**, between "mitigation" and "baseline" under G4 in the 2060s **(b, f)**, between G4 and RCP4.5 under "mitigation" scenario in the 2060s **(c, g)**, and between G4 and RCP8.5 under "mitigation" scenario in the 2060s **(d, h)** based on ISIMIP **(a-d)** and WRF **(e-h)** results. Stippling indicates grid points where differences or changes are not significant at the 5% significant level according to the Wilcoxon signed rank test.

We firstly project the change of $PM_{2.5}$ under G4 and the aerosol mitigation scenario in 2060s relative to 2010s (Fig. 11a, e). Both ISIMIP and WRF project $PM_{2.5}$ decreases in most areas, especially in Tianjin and Langfang, but $PM_{2.5}$ decreases more under ISIMIP than WRF. $PM_{2.5}$ concentration decreases by 6.5 $\mu g/m^3$ over Beijing-Tianjin province in ISIMIP, and decrease by 4.3 μg/m^3 in WRF (Table S2). $PM_{2.5}$ concentration is 0.5-8 μg/m^3 higher in northern Beijing under G4 (“mitigation”) than that during the 2010s in WRF. To show the impact of emission reductions, we compare the $PM_{2.5}$ concentration between aerosol “baseline” and “mitigation” scenarios under G4 in the 2060s (Fig. 11b, 11f), and compare the “mitigation” $PM_{2.5}$ concentration under G4 and the RCP scenarios in the 2060s to clarify the effect of geoengineering compared with climate warming. Compared with “baseline” scenario, $PM_{2.5}$ concentration is less under “mitigation” scenario as expected in both ISIMIP and WRF under G4 (Fig. 11b, 11f), and has a similar spatial pattern with that in Fig. 11a and 11e. Compared with RCP4.5 and RCP8.5, $PM_{2.5}$ concentration under G4 are higher in ISIMIP results (Fig. 11c-11d), but with large differences between the 4 ESMs. G4 $PM_{2.5}$ is simulated greater than in RCP scenarios under HadGEM2-ES and BNU-ESM (Fig. S13k, l, o, p), but there are insignificant differences in most areas under the two MIROC models (Fig. S13c, d, g, h). $PM_{2.5}$ concentrations are larger between G4 and RCP8.5. WRF simulations shows similar changes in $PM_{2.5}$ between G4 and RCPs as ISIMIP (Fig. 11g-h).

3.3.2 $PM_{2.5}$ meteorological and emissions controls in the 2060s

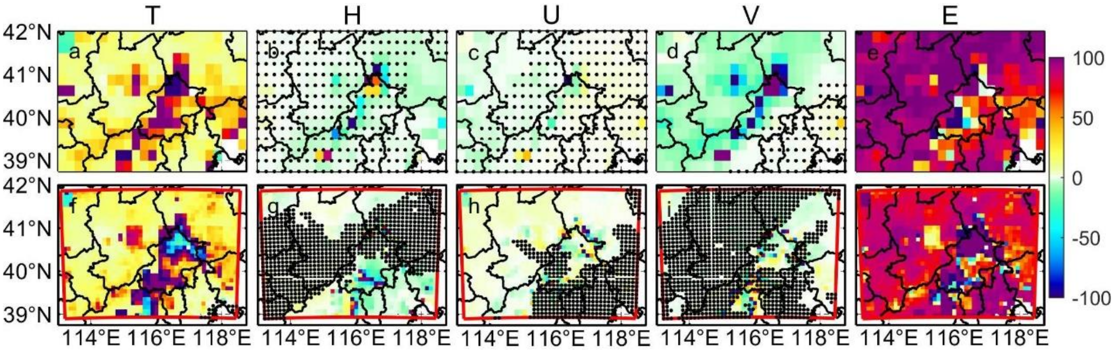

Figure 12. Contribution of climate factors (temperature/T, humidity/H, zonal wind/U, meridional wind/V) and emission (E) to changes in monthly $PM_{2.5}$ concentration ($\Delta PM_{2.5}$) in 2060s under G4 (“mitigation”) relative to 2010s. Top figures **(a-e)** are ISIMIP results, and bottom figures **(f-j)** are WRF results. Stippling indicates the changes are insignificant at the 5% significant level in the Wilcoxon test.

Next, we quantify the contribution of different meteorological factors and $PM_{2.5}$ emissions to $\Delta PM_{2.5}$ between G4 (“mitigation”) in the 2060s and the 2010s (Fig. 12). Both ISIMIP and WRF results show that the increase of temperature and decrease of $PM_{2.5}$ emission play positive roles in reducing $PM_{2.5}$ concentration. ISIMIP results (Fig. 12a-e), suggest that the projected increase of temperature could explain 0-20% of the decrease of $PM_{2.5}$ concentration, and decrease of $PM_{2.5}$ emission could explain more than 90% of changes in $PM_{2.5}$ concentration differences in most of areas. Changes in humidity and westerly winds (positive U-wind) do not cause significant changes in $\Delta PM_{2.5}$, but projected increases southerly wind (positive V-wind) is detrimental to the decrease in $PM_{2.5}$ concentration, and has a 0-10% negative effect on $\Delta PM_{2.5}$ in Zhangjiakou. WRF results show similar spatial pattern in effect of temperature and emission on $\Delta PM_{2.5}$ with ISIMIP results. Although temperature is projected to increase over the whole domain (Fig. S16), there are negative contributions on $\Delta PM_{2.5}$ to the north of Beijing due to increase of $PM_{2.5}$ caused by the negative correlation between $PM_{2.5}$ and its emissions (Fig. S20). The ~1-2% wetter humidity has ~10% negative effect on decrease of $PM_{2.5}$ south of Beijing (Fig. 12g), and 0.2-0.3 m/s deceases of U-wind have 0-10% negative contribution on decrease of $PM_{2.5}$ in Zhangjiakou (Fig. 12h). The changes in each factor in ISIMIP and WRF results are shown in Fig. S15 and Fig. S16, respectively.

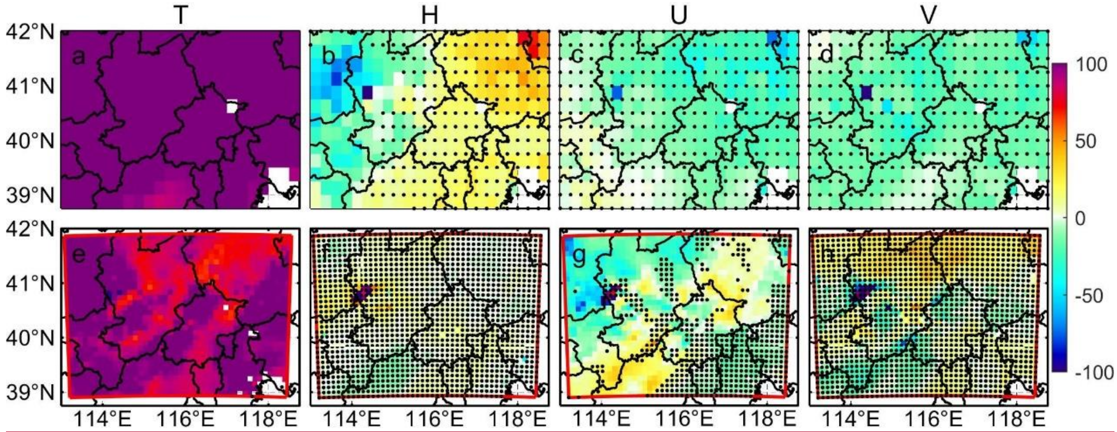

Figure 13. Contribution of climate factors (as in Fig. 12) to changes in monthly $PM_{2.5}$ concentration in 2060s under G4 with aerosol "mitigation" relative to 2060s under RCP4.5 with aerosol "mitigation". Top figures **(a-e)** are ISIMIP results, and bottom figures **(f-j)** are WRF results. Stippling indicates the changes are insignificant at the 5% significant level in the Wilcoxon test.

Now we explore the contribution of each meteorological factor to $\Delta PM_{2.5}$ between G4 ("mitigation") and RCP4.5 ("mitigation") in the 2060s (Fig. 13). The higher $PM_{2.5}$ under G4 is mainly caused by the lower temperature. In ISIMIP, lower temperature explains more than 90% (100% in some places) of the raised $PM_{2.5}$ relative to RCP4.5, although the increase of humidity is also helpful to lower $PM_{2.5}$ in the western domain (Fig. 13a-b). Humidity can increase suspended particle mass and coagulation, promoting deposition (Li et al., 2015). The contribution of differences in U-wind and V-wind on $\Delta PM_{2.5}$ is insignificant (Fig. 13c-d). In WRF, the projected lower temperatures explain more than 70% of the higher $PM_{2.5}$ under G4 relative to RCP4.5 (Fig. 13e). Although the increase of southerly (V) wind contributes 10-20% to the higher $PM_{2.5}$ in the northern domain under HadGEM2-ES and BNU-ESM (Fig. S18), it is insignificant in the ensemble (Fig. 13h). Decreased westerlies (U wind) explains about between +20% and -20% of $PM_{2.5}$ differences (Fig. 13g), since U-wind impacts vary spatially (Fig. S20).

3.3.3 $PM_{2.5}$ impact on health risks now and in the 2060s

Changes in RR of $PM_{2.5}$ for the 5 diseases under the geoengineering and global warming climate scenarios and different emission scenarios during 2060s relative to 2010s for the Beijing-Tianjin province are shown in Fig. 14. Present-day $PM_{2.5}$ related RRs are 1.32 (1.30), 1.37 (1.35), 1.46 (1.43), 1.83 (1.80) and 2.02 (1.99) for chronic obstructive pulmonary disease (COPD), ischemic heart disease (IHD), lung cancer (LC), lung respiratory infection (LRI) and stroke according to the ISIMIP (WRF) simulations (Fig. 14a). RR of LRI is the highest and COPD is the lowest in the five diseases, and WRF estimates of RR are 0.2-0.3 lower than those of ISIMIP. In both the “baseline” and “mitigation” emission scenarios, RRs will be lower under G4, RCP4.5 and RCP8.5 compared with the 2010s. Smaller RR reductions occur under G4 than under RCP4.5 and RCP8.5, and ISIMIP simulates larger reductions than WRF. This is because the $PM_{2.5}$ concentrations from ISIMIP are reduced more than with WRF (Table S2). Under the “baseline” emission scenario (Fig. 14b-d), the biggest reduction of RR for LRI is 0.047 under RCP8.5 in ISIMIP, and RRs for other diseases are projected to reduce by no more than 0.02. Under the “mitigation” emission scenario (Fig. 14e-g), reductions in RRs are 3-6 times greater.

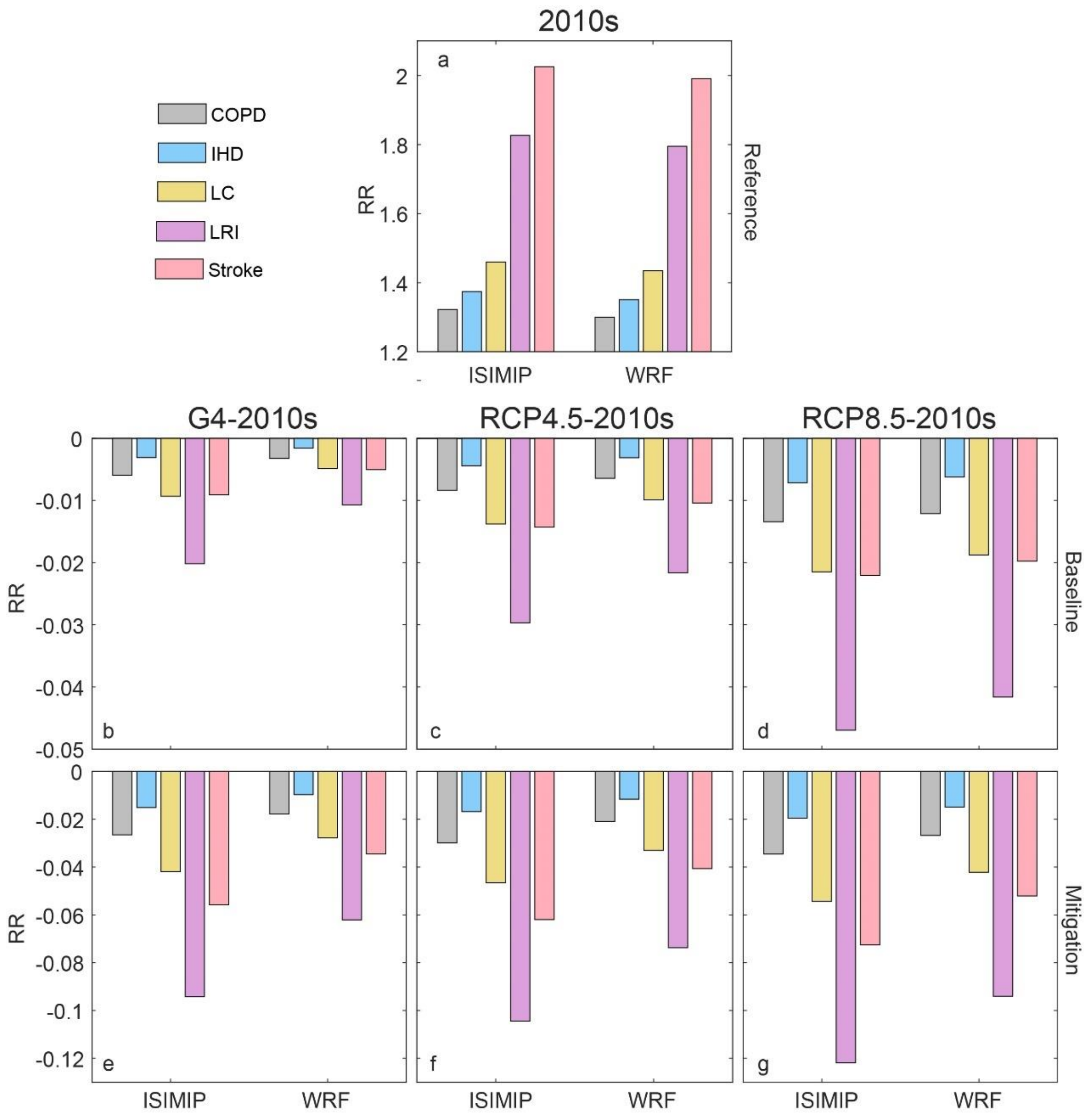

Figure 14. Average population-weighted relative risks of $PM_{2.5}$ related 5 diseases in 2010s **(a)** and its changes between G4 and 2010s **(b, e)**, between RCP4.5 and 2010s **(c, f)** and between RCP8.5 and 2010s **(d, g)** in Beijing-Tianjin province based on the ISIMIP and WRF results, respectively. $PM_{2.5}$ concentration is based on the "baseline" emissions under G4, RCP4,5 and RCP8.5 in the middle 3 figures **(b-d)**, and it is based on the "mitigation" emissions under G4, RCP4,5 and RCP8.5 in the bottom 3 figures **(e-g)**.

4. Discussion

4. ~~and Conclusion~~4.1 Apparent temperature

~~Our study on thermal comfort under geoengineering scenarios for the Beijing megalopolis may be useful across the developing world which is expected to suffer disproportionate climate impact damages relative the global mean, while also undergoing rapid urbanization. Assessing health impacts and mortality due to heat stress under greenhouse gas scenarios should consider urbanization and the change to concrete surfaces from vegetation that leads to differences in heat capacities, rates of evapotranspiration, and hence humidity and apparent temperature. These require downscaled analyses, accurate meteorological and high-resolution land surface datasets.~~

~~In our analysis we assumed the urban area did not change over time, and also that population remains distributed as in the recent past. This may be reasonable in the highly developed and relatively mature greater Beijing-Tianjin region but should be considered in rapidly urbanizing regions elsewhere. But there certainly will be changes over time in the radiative cooling from surface pollution sources. PM2.5 is a health issue in many developing regions (Ran et al., 2022), but as wealth increases efforts to curb air pollution generally clean the air. This has clear health benefits, but also removes aerosols from the troposphere that cool the surface. The urban areas that have higher apparent temperatures at present are also the areas with greatest aerosol load and hence greatest cooling. Once that is removed direct radiation, air temperatures and apparent temperatures will all rise – by several degrees (Wang et al., 2016). So a future more comprehensive health impact study would include both the negative health impacts of aerosol pollution and the potential cooling effects those aerosols produce.~~

Both ISIMIP and WRF can reproduce the observed (~~ERA5~~CN05.1) spatial patterns and seasonal variabilities of apparent temperature in the region around Beijing. WRF shows warm biases in AP during all months relative to ~~ERA5~~ CN05.1 due to warmer temperatures in urban areas, with the exception of ~~driving from the~~ BNU-ESM and HadGEM2-ES ~~in~~ driven summers (Fig. ~~S5~~S8). Both ISIMIP and WRF tend to overestimate population weighted NdAP_32 by ~~46~~370% and ~~116~~590%, respectively. These large discrepancies are due to relatively small overestimates of the likelihood of the tails of the probability distributions which leads to a dramatic increase in the frequency of extreme climate events (Dimri et al., 2018; Huang et al., 2021). AP is about 1.5°C warmer ~~that~~ than 2 m temperature over the Beijing and Tianjin urban areas in summer due to higher vapor pressures amplifying warmer urban temperatures, and this is despite humidity being lower over the cities. Under high humidity conditions, a slight increase in temperature will cause a large increase in heat stress (Li et al., 2018; Luo and Lau, 2019). AP is nearly 4°C colder than 2 m temperature in winter due to wind speed (Fig. 2d). Differences between AP and 2 m temperature (AP-T) during summer are greater in urban areas than neighboring rural areas.

The apparent temperatures in Beijing Tianjin urban areas under G4 in the 2060s are simulated to be 1°C and 2.5°C lower than RCP4.5 and RCP8.5, although AP would be higher than in the recent past. The cooling effect of G4 relative to RCP4.5 and RCP8.5 is greatest under HadGEM2-ES (Fig. ~~S6~~S9, ~~S7~~S10), due to the ESM having largest temperature differences between scenarios (Wang et al., 2022~~ in review~~). WRF downscaling produces reduced seasonality in AP compared with ISIMIP, and WRF produces relatively cooler summers and warmer winters than ISIMIP, and so much less differences in apparent temperature ranges (Fig. ~~10~~15). Differences in AP between G4 and the RCP scenarios are mainly driven by temperature. In all scenarios and downscalings AP rises faster than the temperature due to decreased wind speeds in the future (Li et al., 2018; Zhu et al., 2021) but mainly because of rises in vapor pressure driven by rising temperatures. This effect occurs despite the general drying expected under solar geoengineering (Bala et al., 2008; Yu et al., 2015).

The NdAP_32 under G4 is projected to decrease by 8.6 days per year by ISIMIP and 6.3 days per year by WRF relative to RCP4.5 for Beijing-Tianjin Province. Much larger reductions in NdAP_32 of 33.5 days per year (ISIMIP) and 19.6 days per year (WRF) are projected relative to RCP8.5. Differences between scenarios in frequency of dangerously hot days are far larger using ISIMIP statistical downscaling than using WRF. This is another impact of the reduced seasonality of WRF compared with ISIMIP (Fig. ~~10~~15).

The higher resolution WRF simulation produces a much larger range of apparent temperatures across the domain than ~~ERA5~~ CN05.1 and ISIMIP downscaling. This increased variability makes reaching a statistical significance threshold more challenging for WRF than ISIMIP results. Despite this, the ESM-driven differences in WRF output are less than from ISIMIP, reflecting the physically based processes in the dynamic WRF simulation. This reduces the impact of differences in ESM forcing at the domain boundaries with WRF compared with the statistical bias correction and downscaling methods. Although there are some uncertainties between models and downscaling methods, G4 SAI can not only reduce the mean apparent temperature but also decrease the probability of PDF tails (extreme events) in summer.

822 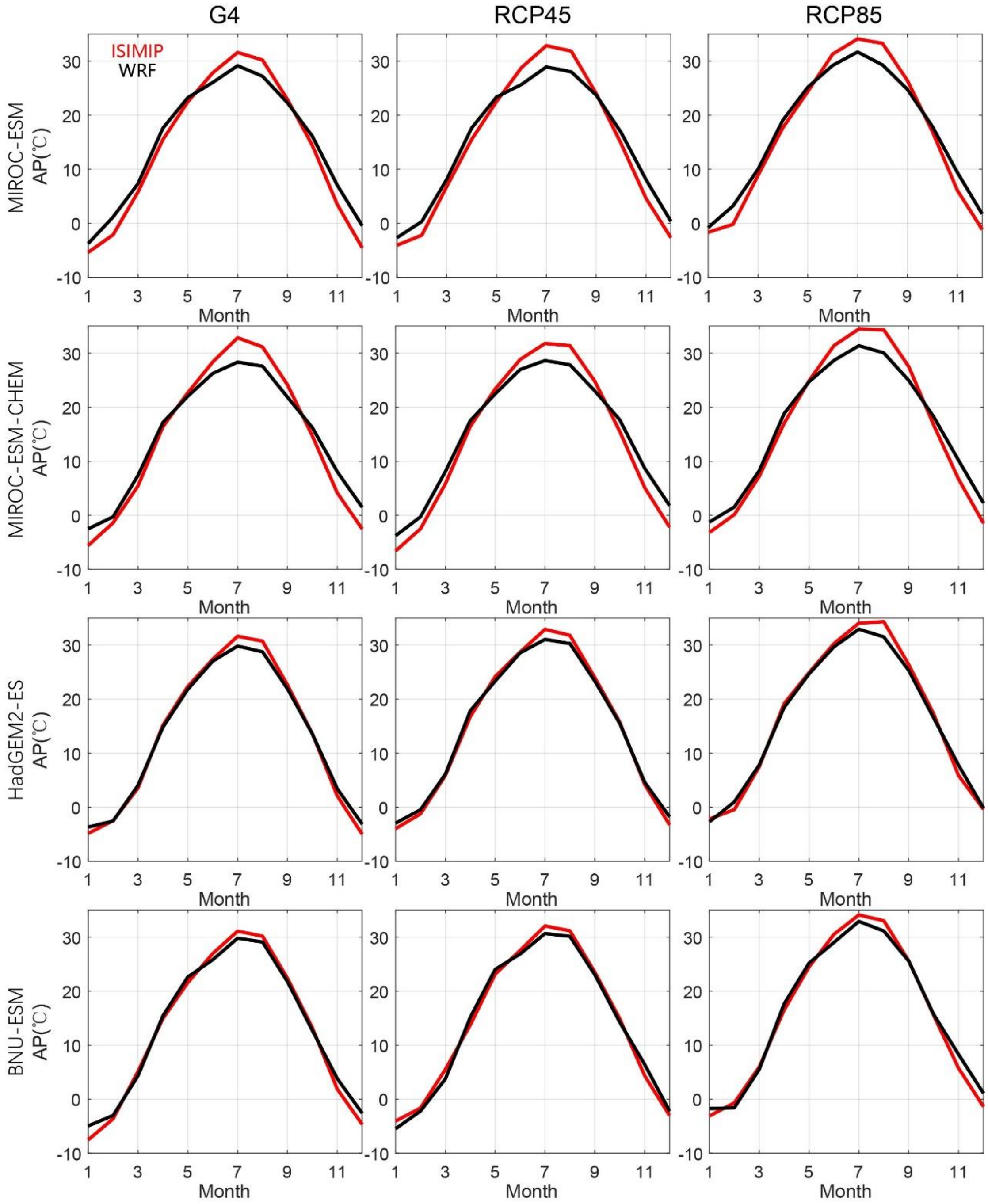
G4
RCP45
RCP85
ISIMIP
WRF
MIROC-ESM
AP(℃)
MIROC-ESM-CHEM
AP(℃)
HadGEM2-ES
AP(℃)
BNU-ESM
AP(℃)
Month

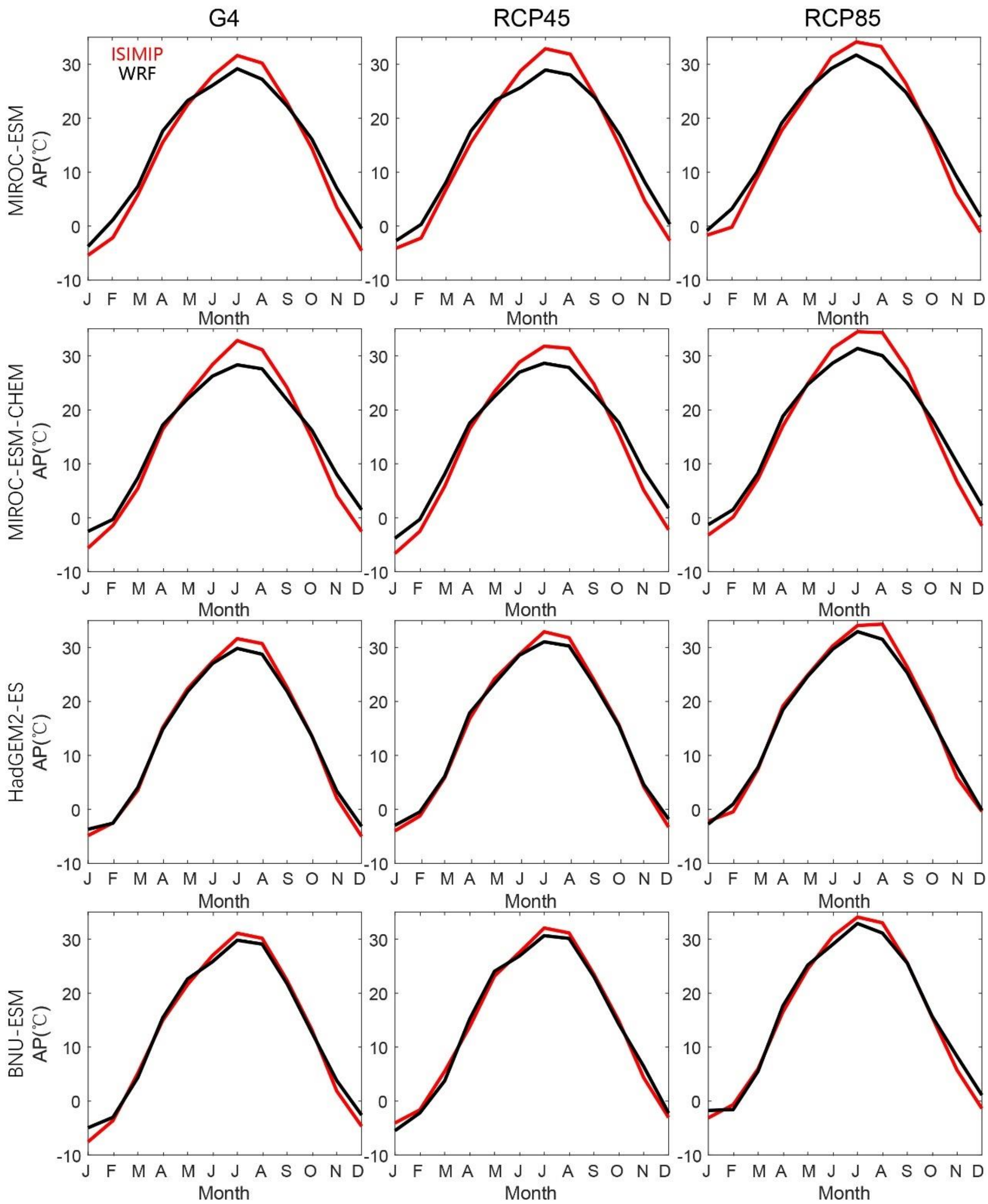

Figure 15~~0~~. Seasonal cycles of apparent temperature from MIROC-ESM, MIROC-ESM-CHEM, HadGEM2-ES and BNU-ESM under G4, RCP4.5 and RCP8.5 in Beijing-Tianjin urban areas during 2060s based on ISIMIP (red) and WRF (black) methods.

4.2 $PM_{2.5}$

We established a set spatially gridded MLR models based on the 4 ESMs downscaled variables under ISIMIP and WRF. The meteorological factors impact $PM_{2.5}$ in complex ways, but the simple spatially gridded MLR models display enough skill to make some illustrative projections of future $PM_{2.5}$ explaining about 70% of the variance during the historical period. $PM_{2.5}$ concentration is correlated with emissions and anti-correlated with temperature in most parts of the domain (Fig, S19-S20). Increased turbulence increases diffusion of $PM_{2.5}$ (Yang et al., 2016), and higher temperatures increase evaporation losses (Liu et al., 2015) of ammonium nitrate (Chuang et al., 2017), and other components (Wang et al., 2006). Humidity may have both positive and negative effects on $PM_{2.5}$ (Chen et al., 2020). It causes more water vapor to adhere to the surface of $PM_{2.5}$, thereby increasing its mass concentration and facilitating aerosol growth (Cheng et al., 2017; Liao et al., 2017). However, when the humidity exceeds a certain threshold, coagulation and particle mass increases rapidly, promoting deposition (Li et al., 2015). So, the slope coefficients between $PM_{2.5}$ and humidity are positive in low humidity areas, including southern plain and the Beijing-Tianjin province, but negative in some northern mountain areas (Fig. S19, S20).

There are large spatial differences in wind speed and direction impacts on $PM_{2.5}$. Yang et al. (2016) found that weaker northerly and westerly winds tend to increase the $PM_{2.5}$ concentration in northern and eastern China, respectively. The effects of wind direction depend on the distribution of emitted $PM_{2.5}$ and the condition of the underlying surface (Chen et al., 2020). Most sources of $PM_{2.5}$ lie to the south of our domain, relatively clean conditions prevail to the north, so northly winds tend to advect clean air, while southerlies bring high concentrations of aerosols. Weak winds tend to increase $PM_{2.5}$ and smog formation due to sinking air and weak diffusion (Su et al., 2017; Yang et al., 2017).

Emissions reductions are expected to play the dominant role in the decrease of $PM_{2.5}$ concentrations under G4 aerosol "mitigation" in 2060s (Fig. 12). Meteorological changes under the different future scenarios make much smaller changes as evidenced by the scenarios using "baseline" – that is present day $PM_{2.5}$ emissions, with decreases in mean annual concentration of 1.0 (1.3), 1.8 (2.0), 3.3 (3.2) $\mu g/m^3$ over Beijing-Tianjin province under G4, RCP4.5 and RCP8.5 with WRF (ISIMIP), (Table S2), which are mainly caused by the temperature increases (Fig. 13). The negative relationships between emission and $PM_{2.5}$ concentration result in the increase of $PM_{2.5}$ under G4 ("mitigation") relative to 2010s in the north of Beijing with WRF. This may be due to changes in $PM_{2.5}$ out of the domain being opposite to those in domain during the MLR fitting period, since relocation of polluting sources from the urban areas mainly to the west, was occurring over the calibration period. The accuracy of $PM_{2.5}$ emission data is also crucial for training MLR models, and $PM_{2.5}$ data was sparse before 2013, relying on reconstructions based on satellite optical depth estimates. Although both increase of temperature and decrease of emission explain more than 90% of the decrease in $PM_{2.5}$ in most areas, there are large spatial differences due to wind and humidity. On the one hand, there is uncertainty in the differences in changes of wind speed and humidity between different ESMs and downscaling methods; on the other hand, the complex physical relationship between them and $PM_{2.5}$ also increases uncertainties. Reductions in $PM_{2.5}$ in the future are projected to decrease $PM_{2.5}$ related health issues, although its effect on different diseases are different. Changes in $PM_{2.5}$ related risk between G4 and RCPs are from 1-3%, with $PM_{2.5}$ emissions policy dominating differences over climate scenario.

Eastham et al. (2018) deduced from experiments using 1 Tg/yr SAI in a coupled chemistry-transport model directly simulating atmospheric chemistry, transport, radiative transfer of UV, emissions, and loss processes, that per unit mass emitted, surface-level emissions of sulfate result in 25 times greater population exposure to $PM_{2.5}$ than emitting the same aerosol into the stratosphere. The G4 experiment specifies 5 Tg/yr injection rate, which over our domain would equate to 1450 t/yr if it was deposited uniformly globally (which it certainly would not be). Reducing this by the 1/25 factor amounts to 58 t/yr which can be compared with present $PM_{2.5}$ emissions of around 3.3×10^5 t/year in our domain. If we consider the aerosol deposition under G4 scenarios, $PM_{2.5}$ concentration will be 0-1 $\mu g/m^3$ higher than that without due to deposition of the SAI aerosols (Fig. S21), and RR is projected to increase by 0.01% for Beijing-Tianjin province (Table S3). This comparison suggests that tropospheric emissions will be much more important for human health in our domain than from the SAI specified by G4.

The most important change in $PM_{2.5}$ will come from emissions reductions, with the different weather conditions under both G4 and RCP scenarios making relatively little practical differences in concentrations. $PM_{2.5}$ concentration is expected to decrease significantly (ISIMIP: -6.5$\mu g/m^3$, WRF: -4.3 $\mu g/m^3$) in the Beijing-Tianjin province, but they will still not meet either Chinese or international standards. The temperature under G4 is lower than that under RCP4.5 and RCP8.5 scenarios, which makes the $PM_{2.5}$ concentration under G4 higher. But the difference in $PM_{2.5}$ between the two is small and even within uncertainty due to projected differences in humidity and wind. Potentially improved estimates from more complex models such as WRF-Chem, CMAQ and GEOS-Chem over the simple MLR methods used here will be of limited value unless the differences between the ESM driving these models is reduced. It can be confirmed that emission policies based on the 13th Five Year Plan are not enough, and higher emission standards need to be developed for a healthy living environment.

5. Conclusion

Our study on thermal comfort and aerosol pollution under geoengineering scenarios for the Beijing megalopolis may be useful across the developing world, which is expected to suffer disproportionate climate impact damages relative the global mean, while also undergoing rapid urbanization. Assessing health impacts and mortality due to heat stress and $PM_{2.5}$ under greenhouse gas scenarios should consider urbanization and the change to concrete surfaces from vegetation that leads to differences in heat capacities, rates of evapotranspiration, and hence humidity and apparent temperature. These require downscaled analyses, accurate meteorological and high-resolution land surface datasets, and industrial development scenarios.

In our analysis we assumed the urban area did not change over time, and also that population remains distributed as in the recent past. This may be reasonable in the highly developed and relatively mature greater Beijing-Tianjin region but should be considered in rapidly urbanizing regions elsewhere. There certainly will be changes over time in the radiative cooling from surface pollution sources. $PM_{2.5}$ is a health issue in many developing regions (Ran et al., 2023), but as wealth increases efforts to curb air pollution generally clean the air. This has clear health benefits, but also removes aerosols from the troposphere that cool the surface. The urban areas that have higher apparent temperatures at present are also the areas with greatest aerosol load and hence greatest cooling. Once that is removed direct radiation, air temperatures and apparent temperatures will all rise – by several degrees (Wang et al., 2016). So, a future more comprehensive health impact study would include both the negative health impacts of aerosol pollution and the potential cooling effects those aerosols produce. Additionally, the formulation of apparent temperature used does not consider the effect of radiation on human comfort (Kong and Huber, 2022). When $PM_{2.5}$ levels are high there is no shade because the sky is milky-white, similarly SAI will brighten the sky (Kravitz et al., 2012). Comfort is increased in clear sky conditions when shade is readily found.

The changes simulated to relative risk from increased $PM_{2.5}$ under the G4 SAI scenario are about 1-3% worse than under RCP4.5, mainly because of lower temperatures under G4. The difference this would make to the overall health burden under SAI depends on the range of other impacts that include changes in apparent temperature we discuss. G4 reduces the number of days with AP>32 (when extreme caution is advised) by 6-8 per year relative to RCP4.5 and by 20-34 relative to RCP8.5. But G4 itself will still increase these extreme caution days by 1-20 relative to conditions in the 2010s. Lowering PM2.5 emissions will increase ground temperatures and the associated risk of dangerous apparent temperatures will also increase rapidly as the distribution of temperatures is shifted making presently rare hot events into much more frequent heat waves.

–

Code and data availability

All ESM data used in this work are available from the Earth System Grid Federation (WCRP, 2021; https://esgf-node.llnl.gov/projects/cmip6, last access: 14 July 2021). The WRF and ISIMIP bias-corrected and downscaled results are available for the authors on request. WRF and ISIMIP codes are freely available at the references cited in the methods sections.

Supplement link

The link to the supplement will be included by Copernicus.

Author contribution

JCM and LZ designed the experiments, JW performed the simulations. All the authors ~~contribute to~~wrote the manuscript.

Competing interests

The authors declare that they have no conflict of interest.

Disclaimer

Publisher's note: Copernicus Publications remains neutral with regard to jurisdictional claims in published maps and institutional affiliations.

Special issue statement:

This article is part of the special issue "Resolving uncertainties in solar geoengineering through multi-model and large-ensemble simulations (ACP/ESD inter-journal SI)". It is not associated with a conference.

Acknowledgements

We thank the editor and two constrictive referees for improving the manuscript. This work relies on the climate modeling groups ~~for~~ participating in the Geoengineering Model Intercomparison Project and their model development teams; the CLIVAR/WCRP Working Group on Coupled Modeling for endorsing the GeoMIP; and the scientists managing the earth system grid data nodes who have assisted with making GeoMIP output available. This research was funded by the National Key Science Program for Global Change Research (2015CB953602).

References

Burnett, R., Pope III, C., Ezzati, M., Olives, C., Lim, S., Mehta, S., Shin, H., Singh, G., Hubbell, B., Brauer, M., Anderson, A., Smith, K., Balmes, J., Bruce, N., Kan, H., Laden, F., Prüss-Ustün, A., Turner, M., Gapstur, S., Diver, W., and Cohen, A.: An

Integrated Risk Function for Estimating the Global Burden of Disease Attributable to Ambient Fine Particulate Matter Exposure, Environ., Health Perspect., 122, 397-403, https://doi.org/10.1289/ehp.1307049, 2014.

Bala, G., Duffy, P. B., Taylor, K. E.: Impact of geoengineering schemes on the global hydrological cycle, Proc. Natl. Acad. Sci. USA, 105 (22), 7664-7669, https://doi.org/10.1073/pnas.0711648105, 2008.

Chen, Z., Chen, D., Kwan, M.-P., Chen, B., Gao, B., Zhuang, Y., Li, R., and Xu, B.: The control of anthropogenic emissions contributed to 80 % of the decrease in $PM_{2.5}$ concentrations in Beijing from 2013 to 2017, Atmos. Chem. Phys., 19, 13519–13533, https://doi.org/10.5194/acp-19-13519-2019, 2019.

Chen, Z., Chen, D., Zhao, C., Kwan, M., Cai, J., Zhuang, Y., Zhao, B., Wang, X., Chen, B., Yang, J., Li, R., He, B., Gao, B., Wang, K., and Xu, B.: Influence of meteorological conditions on $PM_{2.5}$ concentrations across China: A review of methodology and mechanism, Environ. Int., 139, 105558, https://doi.org/10.1016/j.envint.2020.105558, 2020.

Chen, Z., Xie, X., Cai, J., Chen, D., Gao, B., He, B., Cheng, N., and Xu, B.: Understanding meteorological influences on $PM_{2.5}$ concentrations across China: a temporal and spatial perspective, Atmos. Chem. Phys., 18, 5343–5358, https://doi.org/10.5194/acp-18-5343-2018, 2018.

Cheng, L., Meng, F., Chen, L., Jiang, T., and Su, L.: Effects on the haze pollution from autumn crop residue burning over the Jing-Jin-Ji Region, China Environ. Sci., 37, 2801–2812, 2017.

Chi, X., Li, R., Cubasch, U., Cao, W.: The thermal comfort and its changes in the 31 provincial capital cities of mainland China in the past 30 years, Theor. Appl. Climatol., 132(1-2), 599–619, 2018.

Chuang, M., Chou, C., Lin, N., Takami, A., Hsiao, T., Lin, T., Fu, J., Pani, S., Lu, Y., and Yang, T.: A simulation study on $PM_{2.5}$ sources and meteorological characteristics at the northern tip of Taiwan in the early stage of the Asian haze period, Aerosol Air Qual. Res., 17, 3166-3178, https://doi.org/10.4209/aaqr.2017.05.0185, 2017.

Collins, W. J., Bellouin, N., Doutriaux-Boucher, M., Gedney, N., Halloran, P., Hinton, T., Hughes, J., Jones, C. D., Joshi, M., Liddicoat, S., Martin, G., O'Connor, F., Rae, J., Senior, C., Sitch, S., Totterdell, I., Wiltshire, A., Woodward, S.: Development and evaluation of an Earth-System model – HadGEM2, Geosci. Model Dev., 4, 1051–1075, https://doi.org/10.5194/gmd-4-1051-2011, 2011.

Curry, C. L., Sillmann, J., Bronaugh, D., Alterskjaer, K., Cole, J. N. S., Ji, D., Kravitz, B., Kristjánsson, J. E., Moore, J. C., Muri, H., Niemeier, U., Robock, A., Tilmes, S., and Yang, S.: A multimodel examination of climate extremes in an idealized geoengineering experiment, J. Geophys. Res.-Atmos., 119, 3900–3923, https://doi.org/10.1002/2013JD020648, 2014.

Dimri, A. P., Kumar, D., Choudhary, A., Maharana, P.: Future changes over the Himalayas: Maximum and minimum temperature, Global and Planetary Change, 162, 212-234, https://doi.org/10.1016/j.gloplacha.2018.01.015, 2018.

Eastham, D., Weisenstein, D., Keith, D., and Barrett, A.: Quantifying the impact of sulfate geoengineering on mortality from air quality and UV-B exposure, Atmos.

Environ., 187, 424–434. DOI: http://dx.doi.org/10.1016/j.atmosenv.2018.05.047, 2018.

Fan, M., Zhang, Y., Lin, Y., Cao, F., Sun, Y., Qiu, Y., Xing, G., Dao, X., and Fu, P.: Specific sources of health risks induced by metallic elements in $PM_{2.5}$ during the wintertime in Beijing, China, Atmos. Environ., 246, 118112, https://doi.org/10.1016/j.atmosenv.2020.118112, 2021.

Fischer, E., and Knutti, R.: Robust projections of combined humidity and temperature extremes, Nat. Clim. Change, 3, 126-130, https://doi.org/10.1038/nclimate1682, 2013.

Fu, J., Jiang, D., Huang, Y.: 1 km Grid Population Dataset of China, Digital Journal of Global Change Data Repository, https://doi.org/10.3974/geodb.2014.01.06.V1, 2014.

Garcia, F. C., Bestion, E., Warfield, R., Yvon-Durocher, G.: Changes in temperature alter the relationship between biodiversity and ecosystem functioning, Proc. Natl. Acad. Sci. U.S.A., 115, 10989–10999, https://doi.org/10.1073/pnas.1805518115, 2018.

Grinsted, A., Moore, J., and Jevrejeva, S.: Projected Atlantic tropical cyclone threat from rising temperatures, PNAS, 110, 5369-5373, https://doi/10.1073/pnas.1209980110, 2013.

Grundstein, A. and Dowd, J.: Trends in extreme apparent temperatures over the United States, 1949-2010, J. Appl, Meteorol. Climatol., 50(8), 1650–1653, https://doi.org/10.1175/JAMC-D-11-063.1, 2011.

Guan, W., Zheng, X., Chung, K., and Zhong, N.: Impact of air pollution on the burden of chronic respiratory diseases in China: time for urgent action, Lancet, 388, 1939-1951, https://doi.org/10.1016/S0140-6736(16)31597-5, 2016.

Han, J., Wang, J., Zhao, Y., Wang, Q., Zhang, B., Li, H., and Zhai, J.: Spatio-temporal variation of potential evapotranspiration and climatic drivers in the Jing-Jin-Ji region, North China, Agric. For. Meteorol., 256, 75-83, https://doi.org/10.1016/j.agrformet.2018.03.002, 2018.

Hempel, S., Frieler, K., Warszawski, L., Schewe, J., and Piontek, F.: A trend-preserving bias correction – the ISI-MIP approach, Earth Syst. Dynam., 4, 219–236, https://doi.org/10.5194/esd-4-219-2013, 2013.

Hersbach, H., Bell, B., Berrisford, P., Biavati, G., Horányi, A., Muñoz Sabater, J., Nicolas, J., Peubey, C., Radu, R., Rozum, I., Schepers, D., Simmons, A., Soci, C., Dee, D., Thépaut, J-N.: ERA5 hourly data on pressure levels from 1979 to present, Copernicus Climate Change Service (C3S) Climate Data Store (CDS), https://doi.org/10.24381/cds.bd0915c6, 2018.

~~Hersbach, H., Bell, B., Berrisford, P., Biavati, G., Horányi, A., Muñoz Sabater, J., Nicolas, J., Peubey, C., Radu, R., Rozum, I., Schepers, D., Simmons, A., Soci, C., Dee, D., Thépaut, J-N.: ERA5 hourly data on pressure levels from 1979 to present, Copernicus Climate Change Service (C3S) Climate Data Store (CDS), https://doi.org/10.24381/cds.bd0915c6, 2018.~~

Ho, H. C., Knudby, A., Xu, Y., Hodul, M., Aminipouri, M.: A comparison of urban heat islands mapped using skin temperature, air temperature, and apparent temperature

(Humidex), for the greater Vancouver area, Science of The Total Environment, 544, 929-938, https://doi.org/10.1016/j.scitotenv.2015.12.021, 2016.
Huang, J., Li, Q., Song, Z.: Historical global land surface air apparent temperature and its future changes based on CMIP6 projections, Science of The Total Environment, 816, 151656, https://doi.org/10.1016/j.scitotenv.2021.151656, 2021.
IPCC, 2021. Climate change 2021: the physical science basis. In: Masson-Delmotte, V., Zhai, P., Pirani, A., Connors, S.L., Péan, C., Berger, S., Caud, N., Chen, Y., Goldfarb, L., Gomis, M.I., Huang, M., Leitzell, K., Lonnoy, E., Matthews, J.B.R., Maycock, T.K., Waterfifield, T., Yelekçi, O., Yu, R., B.Z. (Eds.), Contribution of Working Group I to the Sixth Assessment Report of the Intergovernmental Panel on Climate Change. Cambridge University Press In Press.
Jacobs, S. J., Pezza, A. B., Barras, V., Bye, J., Vihma, T.: An analysis of the meteorological variables leading to apparent temperature in Australia: present climate, trends, and global warming simulations, Glob. Planet. Chang., 107, 145–156, 2013.
Janssens-Maenhout, G., Crippa, M., Guizzardi, D., Dentener, F., Muntean, M., Pouliot, G., Keating, T., Zhang, Q., Kurokawa, J., Wankmüller, R., Denier van der Gon, H., Kuenen, J. J. P., Klimont, Z., Frost, G., Darras, S., Koffi, B., and Li, M.: HTAP_v2.2: a mosaic of regional and global emission grid maps for 2008 and 2010 to study hemispheric transport of air pollution, Atmos. Chem. Phys., 15, 11411-11432, https://doi.org/10.5194/acp-15-11411-2015, 2015.
Ji, D., Fang, S., Curry, C. L., Kashimura, H., Watanabe, S., Cole, J. N. S., Lenton, A., Muri, H., Kravita, B., Moore, J. C.: Extreme temperature and precipitation response to solar dimming and stratospheric aerosol geoengineering, Atmospheric Chemistry and Physics, 18, 10133-10156, https://doi.org/10.5194/acp-18-10133-2018, 2018.
Ji, D., Wang, L., Feng, J., Wu, Q., Cheng, H., Zhang, Q., Yang, J., Dong, W., Dai, Y., Gong, D., Zhang, R.-H., Wang, X., Liu, J., Moore, J. C., Chen, D., and Zhou, M.: Description and basic evaluation of Beijing Normal University Earth System Model (BNU-ESM) version 1, Geosci. Model Dev., 7, 2039–2064, https://doi.org/10.5194/gmd-7-2039-2014, 2014.
Jin, H., Chen, X., Zhong, R., and Liu, M.: Influence and prediction of $PM_{2.5}$ through multiple environmental variables in China, Sci. Total Enviro., 849, 157910, https://doi.org/10.1016/j.scitotenv.2022.157910, 2022.
Jones, A. C., Hawcroft, M. K., Haywood, J. M., Jones, A., Guo, X., Moore, J.C.: Regional climate impacts of stabilizing global warming at 1.5 K using solar geoengineering, Earth's Future, 6, https://doi.org/10.1002/2017EF000720, 2018.
Kim, D. H., Shin, H. J., Chung, I. U.: Geoengineering: Impact of marine cloud brightening control on the extreme temperature change over East Asia, Atmosphere, 11(12), 1345, https://doi.org/10.3390/atmos11121345, 2020.
Klimont, Z., Kupiainen, K., Heyes, C., Purohit, P., Cofala, J., Rafaj, P., Borken-Kleefeld, J., and Schöpp, W.: Global anthropogenic emissions of particulate matter including black carbon, Atmos. Chem. Phys., 17, 8681–8723, https://doi.org/10.5194/acp-17-8681-2017, 2017.

Kong, Q., and Huber, M.: Explicit calculations of wet-bulb globe temperature compared with approximations and why it matters for labor productivity, Earth's Future, 10, e2021EF002334, https://doi.org/10.1029/2021EF002334, 2022.

Kraaijenbrink, P. D. A., Bierkens, M. F. P., Lutz A. F., Immerzeel, W. W.: Impact of a global temperature rise of 1.5 degrees Celsius on Asia's glaciers, Nature, 549, 257-260, https://doi.org/10.1038/nature23878, 2017.

Kravitz, B., MacMartin, D., and Caldeira, K.: Geoengineering: Whiter skies?, Geophys. Res. Lett., 39, L11801, https://doi.org/10.1029/2012GL051652, 2012.

Kravitz, B., Robock, A., Boucher, O., Schmidt, H., Taylor, K. E., Stenchikov, G., and Schulz, M.: The geoengineering model intercomparison project (GeoMIP), Atmos. Sci. Lett., 12(2), 162-167, https://doi.org/10.1002/asl.316, 2011.

Kuswanto, H., Kravitz, B., Miftahurrohmah, B., Fauzi, F., Sopahaluwaken, A., and Moore, J. C.: Impact of solar geoengineering on temperatures over the Indonesian Maritime Continent, Int. J. Climatol., 1-20, https://doi.org/10.1002/joc.7391, 2021.

Lee, C. and Sheridan, S.: A new approach to modeling temperature-related mortality: non-linear autoregressive models with exogenous input, Environ. Res., 164:53–64, https://doi.org/10.1016/j.envres.2018.02.020, 2018.

Lenton, T. and Vaughan, N.: The radiative forcing potential of different climate geoengineering options, Atmos. Chem. Phys., 9, 5539–5561, https://doi.org/10.5194/acp-9-5539-2009, 2009.

Li, D., Wu, Q., Feng, J., Wang, Y., Wang, L., Xu, Q., Sun, Y., Cao, K., and Cheng, H.: The influence of anthropogenic emissions on air quality in Beijing-Tianjin-Hebei of China around 2050 under the future climate scenario, J. Cleaner Prod., 388, 135927, https://doi.org/10.1016/j.jclepro.2023.135927, 2023.

Li, J., Chen, H., Li, Z., Wang, P., Cribb, M., and Fan, X.: Low-level temperature inversions and their effect on aerosol condensation nuclei concentrations under different large-scale synoptic circulations, Adv. Atmos. Sci., 32, 898-908, https://doi.org/10.1007/s00376-014-4150-z, 2015.

Li, J., Chen, Y., Gan, T., Lau, N.: Elevated increases in human-perceived temperature under climate warming, Nat. Clim. Chang., 8 (1), 43–47, https://doi.org/10.1038/s41558-017-0036-2, 2018.

Li, K., Liao, H., Zhu, J., and Moch, J.: Implications of RCP emissions on future $PM_{2.5}$ air quality and direct radiative forcing over China, J. Geophys. Res. Atmos., 121, 12, 985-13, 008, https:// doi:10.1002/2016JD025623, 2016.

Li, M., Klimont, Z., Zhang, Q., Martin, R. V., Zheng, B., Heyes, C., Cofala, J., Zhang, Y., and He, K.: Comparison and evaluation of anthropogenic emissions of SO_2 and NO_x over China, Atmos. Chem. Phys., 18, 3433–3456, https://doi.org/10.5194/acp-18-3433-2018, 2018.

Liao, T., Wang, S., Ai, J., Gui, K., Duan, B., Zhao, Q., Zhang, X., Jiang, W., and Sun, Y.: Heavy pollution episodes, transport pathways and potential sources of $PM_{2.5}$ during the winter of 2013 in Chengdu (China), Sci. Total Environ., 584–585, 1056–1065, https://doi.org/10.1016/j.scitotenv.2017.01.160, 2017.

Lin, G., Fu, J., Jiang, D., Wang, J., Wang, Q., and Dong, D.: Spatial variation of the relationship between $PM_{2.5}$ concentrations and meteorological parameters in China, BioMed Res. Int., 2015, 684618, https://doi.org/10.1155/2015/684618, 2015.

Luo, M., & Lau, N.-C.: Characteristics of summer heat stress in China during 1979–2014: Climatology and long-term trends, Climate Dynamics, 53(9), 5375–5388, https://doi.org/10.1007/s00382-019-04871-5, 2019.

Luo, M. and Lau, N.: Increasing Human-Perceived Heat Stress Risks Exacerbated by Urbanization in China: A Comparative Study Based on Multiple Metrics, Earth's Future, 9 (7), https://doi.org/10.1029/2020EF001848, 2021.

Lyon, B. and Barnston, A.: Diverse characteristics of US summer heat waves, J. Clim., 30 (19), 7827–7845, https://doi.org/10.1175/JCLI-D-17-0098.1, 2017.

Maji, K., Ye, W., Arora, M., and Nagendra, S.: $PM_{2.5}$-related health and economic loss assessment for 338 Chinese cities, Environ. Int., 121, 392-403, https://doi.org/10.1016/j.envint.2018.09.024, 2018.

Matthews, T., Wilby, R., and Murphy, C.: Communicating the deadly consequences of global warming for human heat stress, PNAS, 114, 3861-3866, https://doi.org/10.1073/pnas.1617526114, 2017.

Mishra, D., Goyal, P., and Upadhyay, A.: Artificial intelligence based approach to forecast $PM_{2.5}$ during haze episodes: a case study of Delhi, India, Atmos. Environ., 102, 239–248, https://doi.org/10.1016/j.atmosenv.2014.11.050, 2015.

Murray, F.: On the computation of saturation vapor pressure, Rand Corp Santa Monica Calif, 1966.

Nguyen, G., Shimadera, H., Uranishi, K., Matsuo, T., and Kondo, A.: Numerical assessment of $PM_{2.5}$ and O_3 air quality in Continental Southeast Asia: Impacts of future projected anthropogenic emission change and its impacts in combination with potential future climate change impacts, Atmos. Environ., 226, 117398, https://doi.org/10.1016/j.atmosenv.2020.117398, 2020.

Perkins, S. and Alexander, L.: On the measurement of heat waves, J Clim., 26 (13), 4500–4517, https://doi.org/10.1175/JCLI-D-12-00383.1, 2013.

Ran, Q., Lee, S., Zheng, D., Chen, H., Yang, S., Moore, J., Dong, W.: Potential Health and Economic Impacts of Shifting Manufacturing from China to Indonesia or India, Science of the total environment, 855, 158634, http://dx.doi.org/10.1016/j.scitotenv.2022.158634, 2022.

Riahi, K., Rao, S., Krey, V., Cho, C., Chirkov, V., Fischer, G., Kindermann, G., Nakicenovic, N., Rafaj, P.: RCP 8.5—A scenario of comparatively high greenhouse gas emissions, Climatic Change 109, 33, https://doi.org/10.1007/s10584-011-0149-y, 2011.

Robock, A., Marquardt, A., Kravitz, B. and Stenchikov, G.: Benefits, risks, and costs of stratospheric geoengineering, Geophys. Res. Lett., 36(19), https://doi.org/10.1029/2009GL039209, 2009.

Shepherd, J.: Geoengineering the climate: Science, governance, and uncertainty, Royal Society Policy document 10/09, 82 pp, 2009.

Song, F., Zhang, G., Ramanathan, V. and Ruby Leung, L.: Trends in surface equivalent potential temperature: A more comprehensive metric for global warming and weather extremes, Proc. Natl. Acad. Sci. U.S.A., 119, 6, https://doi.org/10.1073/pnas.2117832119, 2022.

Steadman, R. G.: A universal scale of apparent temperature, J. Appl. Meteorol., 23 (12), 1674–1687, https://doi.org/10.1175/1520-0450(1984)023<1674:AUSOAT>2.0.CO;2, 1984.

Steadman, R. G.: Norms of apparent temperature in Australia, Aust. Meteorol. Mag., 43, 1–16, 1994.

Stohl, A., Aamaas, B., Amann, M., Baker, L. H., Bellouin, N., Berntsen, T. K., Boucher, O., Cherian, R., Collins, W., Daskalakis, N., Dusinska, M., Eckhardt, S., Fuglestvedt, J. S., Harju, M., Heyes, C., Hodnebrog, Ø., Hao, J., Im, U., Kanakidou, M., Klimont, Z., Kupiainen, K., Law, K. S., Lund, M. T., Maas, R., MacIntosh, C. R., Myhre, G., Myriokefalitakis, S., Olivié, D., Quaas, J., Quennehen, B., Raut, J.-C., Rumbold, S. T., Samset, B. H., Schulz, M., Seland, Ø., Shine, K. P., Skeie, R. B., Wang, S., Yttri, K. E., and Zhu, T.: Evaluating the climate and air quality impacts of short-lived pollutants, Atmos. Chem. Phys., 15, 10529–10566, https://doi.org/10.5194/acp-15-10529-2015, 2015.

Su, J., Brauer, M., Ainslie, B., Steyn, D., Larson, T., and Buzzelli, M.: An innovative land use regression model incorporating meteorology for exposure analysis, Sci. Total Environ., 390, 520-529, https://doi.org/10.1016/j.scitotenv.2007.10.032, 2008.

Tong, C., Yim, S., Rothenberg, D., Wang, C., Lin, C., Chen, Y., and Lau, N.: Projecting the impacts of atmospheric conditions under climate change on air quality over the Pearl River Delta region, Atmos. Environ., 193, 79-87, https://doi.org/10.1016/j.atmosenv.2018.08.053, 2018.

Torma, C. and Giogi, F.: Assessing the contribution of different factors in regional climate model projections using the factor separation method, Atmos. Sci. Lett., 15, 239–244, https://doi.org/10.1002/asl2.491, 2014.

Upadhyay, A., Dey, S., Goyal, P., and Dash, S.: Projection of near-future anthropogenic $PM_{2.5}$ over India using statistical approach, Atmos. Environ., 186, 178-188, https://doi.org/10.1016/j.atmosenv.2018.05.025, 2018.

Vandyck, T., Keramidas, K., Saveyn, B., et al.: A global stocktake of the Paris pledges: Implications for energy systems and economy, Global Environmental Change, 41, 46-63, https://doi.org/10.1016/j.gloenvcha.2016.08.006, 2016.

Wang, J., Allen, D., Pickering, K., Li, Z., He, H.: Impact of aerosol direct effect on East Asian air quality during the EAST-AIRE campaign, J. Geophys. Res.- Atmos., 121, 6534-6554, https://doi.org/10.1002/2016JD025108, 2016.

Wang, J., Moore, J. C., Zhao, L., Yue, C., and Di, Z.: Regional dynamical and statistical downscaling temperature, humidity and windspeed for the Beijing region under stratospheric aerosol injection geoengineering, Earth Syst. Dynam~~.~~ ~~Discuss.~~ .,~~[preprint],~~ https://doi.org/10.5194/esd-2022-35, ~~in review,~~ 2022.

Wang, J., Feng, J., Yan, Z., Hu, Y., and Jia, G.: Nested high-resolution modeling of the impact of urbanization on regional climate in three vast urban agglomerations in China, J. Geophys. Res.- Atmos., 117(D21), https://doi.org/10.1029/2012JD018226, 2017.

Wang, J., Zhang, L., Niu, X., and Liu, Z.: Effects of $PM_{2.5}$ on health and economic loss:

Evidence from Beijing-Tianjin-Hebei region of China, J. Cleaner Prod., 257, 120605, https://doi.org/10.1016/j.jclepro.2020.120605, 2020.

Wang, P., Luo, M., Liao, W., Xu, Y., Wu, S., Tong, X., Tian, H., Xu, F., Han, Y.: Urbanization contribution to human perceived temperature changes in major urban agglomerations of China, Urban Climate, 38, 100910, https://doi.org/10.1016/j.uclim.2021.100910, 2021.

Wang, S., Ancell, B., Huang, G., Baetz, B.: Improving robustness of hydrologic ensemble predictions through probabilistic pre- and post-processing in sequential data assimilation, Water Resources Research, 54, 2129–2151, https://doi.org/10.1002/2018WR022546, 2018.

Wang, X., Huang, G., Lin, Q., Nie, X., Cheng, G., Fan, Y., Li, Z., Yao, Y., Suo, M.: A stepwise cluster analysis approach for downscaled climate projection - a Canadian case study, Environ. Model Softw., 49, 141–151, https://doi.org/10.1016/j.envsoft.2013.08.006, 2013.

Wang, Y., Chen, L., Song, Z., Huang, Z., Ge, E., Lin, L., Luo, M.: Human-perceived-temperature changes over South China: long-term trends and urbanization effects, Atmos. Res., 215, 116–127, https://doi.org/10.1016/j.atmosres.2018.09.006, 2019.

Wang, Y., Yao, L., Wang, L., Liu, Z., Ji, D., Tang, G., Zhang, J., Sun, Y., Hu, N., and Xin, J.: Mechanism for the formation of the January 2013 heavy haze pollution episode over central and eastern China, Sci. China Earth Sci., 57, 14-25, https://doi.org/10.1007/s11430-013-4773-4, 2014.

Wang, Y., Zhuang, G., Zhang, X., Huang, K., Xu, C., Tang, A., Chen, J., and An, Z.: The ion chemistry, seasonal cycle, and sources of $PM_{2.5}$ and TSP aerosol in Shanghai, Atmos. Environ., 40, 2935-2952, https://doi.org/10.1016/j.atmosenv.2005.12.051, 2006.

Watanabe, S., Hajima, T., Sudo, K., Nagashima, T., Takemura, T., Okajima, H., Nozawa, T., Kawase, H., Abe, M., Yokohata, T., Ise, T., Sato, H., Kato, E., Takata, K., Emori, S., and Kawamiya, M.: MIROC-ESM 2010: model description and basic results of CMIP5-20c3m experiments, Geosci. Model Dev., 4, 845–872, https://doi.org/10.5194/gmd-4-845-2011, 2011.

Wei, J., Li, Z., Lyapustin, A., Sun, L., Peng, Y., Xue, W., Su, T., and Cribb, M.: Reconstructing 1-km-resolution high-quality $PM_{2.5}$ data records from 2000 to 2018 in China: spatiotemporal variations and policy implications, Remote Sens. Environ., 252, 112136, https://doi.org/10.1016/j.rse.2020.112136, 2021.

Wilcke, R. A. I., Mendlik, T., Gobiet, A.: Multi-variable error correction of regional climate models, Clim. chang., 120(4), 871-887, https://doi.org/10.1007/s10584-013-0845-x, 2013.

Wu, J., Gao, X., Giorgi, F., Chen, D.: Changes of effective temperature and cold/hot days in late decades over China based on a high resolution gridded observation dataset, Int. J. Climatol., 37:788–800, https://doi.org/10.1002/joc.5038, 2017.

Wu, J., Gao, X., Giorgi, F., Chen, D.: Changes of effective temperature and cold/hot days in late decades over China based on a high resolution gridded observation dataset, Int. J. Climatol., 37:788–800, https://doi.org/10.1002/joc.5038, 2017.

Xue, W., Zhang, J., Zhong, C., Li, X., and Wei, J.: Spatiotemporal $PM_{2.5}$ variations and its response to the industrial structure from 2000 to 2018 in the Beijing-Tianjin-Hebei region, J. Cleaner Prod., 279, 123742, https://doi.org/10.1016/j.jclepro.2020.123742, 2021.

Yang, S., Ma, Y., Duan, F., He, K., Wang, L., Wei, Z., Zhu, L., Ma, T., Li, H., Ye, S.: Characteristics and formation of typical winter haze in Handan, one of the most polluted cities in China, Sci. Total Environ., 613-614, 1367-1375, https://doi.org/10.1016/j.scitotenv.2017.08.033, 2018.

Yang, X., Zhao, C., Guo, J., and Wang, Y.: Intensification of aerosol pollution associated with its feedback with surface solar radiation and winds in Beijing, J. Geophys. Res. Atmos., 121, 4093-4099, https://doi.org/10.1002/2015JD024645, 2016.

Yang, Y., Maraun, D., Ossó, A., and Tang, J.: Increased spatial extent and likelihood of compound long-duration dry and hot events in China, 1961–2014, Nat. Hazards Earth Syst. Sci., 23, 693–709, https://doi.org/10.5194/nhess-23-693-2023, 2023.

Yang, Y., and Tang, J.: Substantial Differences in Compound Long - Duration Dry and Hot Events Over China Between Transient and Stabilized Warmer Worlds at 1.5° C Global Warming, Earths Future, 11, e2022EF002994, https://doi.org/10.1029/2022EF002994, 2023.

Yang, Y., Tang, J., Xiong, Z., Wang, S., and Yuan, J.: An intercomparison of multiple statistical downscaling methods for daily precipitation and temperature over China: future climate projections, Clim. Dynam., 52, 6749–6771, https://doi.org/10.1007/s00382-018-4543-2, 2019.

Yu, X., Moore, J. C., Cui, X., Rinke, A., Ji, D., Kravitz, B., and Yoon, J.: Impacts, effectiveness and regional inequalities of the GeoMIP G1 to G4 solar radiation management scenarios, Global and Planetary Change, 129, 10-22, https://doi.org/10.1016/j.gloplacha.2015.02.010, 2015.

Zhan, P., Zhu, W., Zhang, T., Cui, X., Li, N.: Impacts of sulfate geoengineering on rice yield in China: Results from a multimodel ensemble, Earth's Future, 7(4), 395-410, https://doi.org/10.1029/2018EF001094, 2019.

Zhang, Q., Zheng, Y., Tong, D., Shao, M., Wang, S., Zhang, Y., Xu, X., Wang, J., He, H., Liu, W., Ding, Y., Lei, Y., Li, J., Wang, Z., Zhang, X., Wang, Y., Cheng, J., Liu, Y., Shi, Q., Yan, L., Geng, G., Hong, C., Li, M., Liu, F., Zheng, B., Cao, J., Ding, A., Gao, J., Fu, Q., Huo, J., Liu, B., Liu, Z., Yang, F., He, K., and Hao, J.: Drivers of improved $PM_{2.5}$ air quality in China from 2013 to 2017, PNAS, 116, 24463-24469, https://doi.org/10.1073/pnas.1907956116, 2019.

Zhang, Z., Gong, D., Mao, R., Kim, S., Xu, J., Zhao, X., and Ma, Z.: Cause and predictability for the severe haze pollution in downtown Beijing in November–December 2015, Sci. Total Enviro., 592, 627-638, https://doi.org/10.1016/j.scitotenv.2017.03.009, 2017.

Zhao, D., Xin, J., Gong, C., Quan, J., Liu, G., Zhao, W., Wang, Y., Liu, Z., and Song, T.: The formation mechanism of air pollution episodes in Beijing city: insights into the measured feedback between aerosol radiative forcing and the atmospheric boundary layer stability, Sci. Total Environ., 692, 371–381, https://doi.org/10.1016/j.scitotenv.2019.07.255, 2019.

Zhou, B., Xu, Y., Wu, J., Dong, S., and Shi, Y.: Changes in temperature and precipitation extreme indices over China: analysis of a high-resolution grid dataset, Int. J. Climatol., 36, 1051–1066, https://doi.org/10.1002/joc.4400, 2016.

Zhu, J., Wang, S., Huang, G.: Assessing Climate Change Impacts on Human-Perceived Temperature Extremes and Underlying Uncertainties, Journal of Geophysical Research: Atmosphere, 124 (7), 3800-3821, https://doi.org/10.1029/2018JD029444, 2019.

Zhu, X., Huang, G., Zhou, X., Zheng, S.: Projection of apparent temperature using statistical downscaling approach in the Pearl River Delta, Theor. Appl. Climatol., 144 (3–4), 1253–1266, https://doi.org/10.1007/s00704-021-03603-2, 2021.